NASA Contractor Report 177514

Solid State Photomultiplier for Astronomy Phase II

P. J. Besser
K. M. Hays
R. A. LaViolette

CONTRACT NAS2-12400
May 1989

National Aeronautics and
Space Administration

NASA Contractor Report 177514

Solid State Photomultiplier for Astronomy Phase II

P. J. Besser
K. M. Hays
R. A. LaViolette

Rockwell International Science Center, Anaheim, California

Prepared for
Ames Research Center
CONTRACT NAS2–12400
May 1989

National Aeronautics and
Space Administration

Ames Research Center
Moffett Field, California 94035

TABLE OF CONTENTS

LIST OF ILLUSTRATIONS

TABLES

1.0 SUMMARY

Epitaxial layers with varying donor concentration profiles were grown on silicon substrate wafers using chemical vapor deposition (CVD) techniques, and Solid State Photomultiplier (SSPM) devices were fabricated from the wafers. Representative detectors were tested in a low background photon flux, low temperature environment to determine the device characteristics for comparison to NASA goals for astronomical applications. SSPM temperatures varied between 6 and 11 K with background fluxes in the range from $< 5 \times 10^{6}$ to 10^{13} photons/cm^{2}-s at wavelengths of 3.2 and 20 um. Measured parameters included quantum efficiency, dark count rate and bias current. Temperature for optimal performance is 10 K, the highest ever obtained for SSPMs. The devices exhibit a combination of the lowest dark current and highest quantum efficiency yet achieved. Experimental data were reduced, analyzed and used to generate recommendations for future studies.

The background and present status of the microscopic theory of SSPM operation were reviewed and are summarized. Present emphasis is on modeling of the avalanche process which is the basis for SSPM operation. Approaches to the solution of the Boltzmann transport equation are described and the treatment of electron scattering mechanisms is presented. The microscopic single-electron transport theory is ready to be implemented for large-scale computations. Future work will be directed towards simulation of the multi-electron theory, improvement of the neutral-impurity scattering theory and consideration of other scattering mechanisms.

2.0 INTRODUCTION

Rockwell International's Solid State Photomultiplier (SSPM)[1] is an impurity-band avalanche device which can count individual photons with wavelengths between 0.4 and 28 um.[2] Its response to a photon is a pulse of between 10^4 and 10^5 conduction electrons, making it an important device for use in low-background, infrared (IR) detection applications. The SSPM is, however, a new device which must be better understood before it is incorporated into a system.

The characteristics of the SSPM make it a potentially important device for use in astronomical applications. Contract NAS2-12400 was initiated in June 1986 to conduct analytical modeling and characterization of the SSPM to provide a basis for assessing its use in astronomical systems. The first phase of the contract ended on June 30, 1987, and the results of that effort are contained in NASA Contract Report CR177465.[3]

The second phase of the contract began on September 30, 1987, and involved the computation of device simulations, fabrication of SSPM devices with improved characteristics and preliminary characterization of the improved devices. This report discusses results of the theoretical (Section 3.0) and experimental efforts (Section 4.0) to develop an improved understanding of SSPM operation and its potential for use in astronomical applications.

Conclusions drawn from the results and recommendations for future work are contained in Section 5.0.

3.0 SSPM DEVICE MODELING

3.1 BACKGROUND

The goal of the SSPM modeling effort is the prediction of device performance from design parameters and operating conditions. Table I lists the major parameters which characterize SSPM performance along with the design parameters and operating conditions which control the device performance. Model development interacts with the experimental device development in an iterative manner. Predictions of the initial model are compared with device data and the results are used to modify and improve the model. If sufficiently good agreement is obtained between the theoretical and experimental results, the model can then be used to predict device performance under a variety of design and operating conditions to reduce the amount of time-consuming and expensive fabrication and testing required for device optimization.

Development of a microscopic theory for SSPM device operation requires first, the formulation of the theory and second, the solution of the resulting equations, whose complexity requires computational solutions. Formulation of the theory in terms of the single-electron Boltzmann equation and its translation into efficient computer code is being pursued on another program.[4] The computations required to model the SSPM with this approach are most effectively carried out on vectorizing supercomputers, such as the NASA-Ames Research Center (ARC) CRAY-XMP. Therefore, the work on this task is aimed at providing the solution of the Boltzmann equation for single-electron transport in arsenic-doped silicon-based

Table I. SSPM Model Parameters

Performance Parameters	Design Parameters
Gain	Geometry
Gain Dispersion	Impurity Concentration
Speed	Impurity Type
Noise	Impurity Distribution
Quantum Efficiency	
Detectivity	Operating Conditions
Bandwidth	Applied Bias
Dynamic Range, Saturation	Temperature
	Photon Flux

SSPMs responding to infrared radiation, using programs optimized for NASA supercomputers. The solution will, in turn, provide parameters required as input to the phenomenological theory developed earlier on this contract.[3][5]

The remainder of this introduction will present an outline of SSPM theory and its goals. The microscopic theory based on the Boltzmann equation is discussed in the next section followed by a consideration of the requirements for efficient computation. In the concluding section, the current status of the work is summarized and recommendations for future work are made.

Several of the most important aspects of SSPM performance (e.g., gain, quantum efficiency, speed, breakdown, and noise) depend directly on the microscopic dynamics of the charge carriers in the device, especially in the gain region, where a sub-breakdown carrier avalanche is generated via the impact-ionization of neutral impurities by the carriers.[2] The carrier dynamics are, in turn, sensitive to device geometry, impurity profiles, and external electric fields. Unfortunately, since experiments cannot yet provide a detailed probe of carrier dynamics, the avalanche mechanism so important to SSPM performance is not understood at the required level of detail. Therefore, a detailed model of the SSPM must be developed in order to predict the consequences of design variations for device performance. In particular, the theory for the SSPM concentrates on electron transport in the gain region.[6] The theory began along phenomenological lines, and continues in a microscopic treatment, as reviewed below.

Earlier work on this contract[3] demonstrated that qualitative features of the electron pulse height distribution which results from photo-initiated avalanches in the SSPM can be predicted from a one-dimensional stochastic branching process. This distribution yields the gain, gain dispersion, and other relevant moments related to the gain. Of course, this model does not provide direct dynamical information; e.g., the model neglects variations in the electric field with time or space. This phenomenological treatment requires, in addition to the impurity profile and device geometry, the following parameters as inputs: impact-ionization rate, minimum distance required for a carrier to travel to acquire the impact-ionization threshold energy, and the distribution (or its moments) of distances between respective impact-ionization events. The required parameters are not presently available from experiments. Therefore, apart from reasonable guesses, it is necessary to turn to a microscopic electron transport theory to supply these parameters and to expand insight into fundamental device processes.

The microscopic electron dynamics for the SSPM are modeled with the semiclassical Boltzmann equation. Since the conditions of avalanche growth are far from equilibrium, the versatility of this approach is crucial. This transport equation describes the dynamics by providing, as its solution, the probability that an electron has a momentum and a position for any specified time. Both stationary and transient

dynamical properties (e.g., current, mobility) may be found through the appropriate averages taken with the dynamical momentum-position distribution. Furthermore, both the electric field (as a function of time and position) and the electron mobilities can be calculated and used to predict the gain and its dispersion, as well as the breakdown voltage and current.

Two kinds of solutions of the Boltzmann equation are anticipated. The direct simulation of avalanche dynamics ordinarily requires solution of the Boltzmann equation for all of the many electrons generated in the avalanche. While this multi-carrier solution is required and planned for future work, the current modeling effort is devoted to a single-carrier solution. Although the single-carrier solution cannot directly simulate the dynamics of avalanche development, it should provide input parameters for the phenomenological theory. Subsequent development of the avalanche can then be modeled by the branching process discussed above to yield the gain and gain dispersion.

The Boltzmann equation and its solution are discussed in more detail in the following section.

3.2 MICROSCOPIC TRANSPORT THEORY

The Boltzmann equation provides f(p,r,t), the probability that an electron at time t is found at position r with momentum p. This single-electron distribution function yields transport properties through its various contractions and moments. For example, the carrier concentration n(r,t) is the contraction $\int dp/4\pi^3\, f(p,r,t)$. The Boltzmann equation for f may be written as[7]

$$\left[\frac{\partial}{\partial t} + \dot{p}\,\frac{\partial}{\partial p} + \dot{r}\,\frac{\partial}{\partial r}\right] f(p,r,t) = \left(\frac{V_o}{8\pi^3}\right) \int dp' \sum_{\alpha} W_{\alpha}(p \rightarrow p')$$

$$[f(p',r,t) - f(p,r,t)], \qquad (1)$$

which shows that the input required for the Boltzmann equation consists of the probabilities (per unit time) $W_{\alpha}(p \rightarrow p')$ that an electron with momentum p acquires a new momentum p' by one of the scattering mechanisms (labeled α), and the equation of motion which defines $\dot{p}$ and $\dot{r}$. The semi-classical equation of motion for an electron at r with momentum p is[7]

$$\dot{r} = \partial E(p)/\partial p, \quad \dot{p} = F(r) + F^{ext}(r), \qquad (2)$$

where $F^{ext}(r)$ is the force due to the external electric field, $F(r)$ is the force (if any) on the electron due to other charges, and $E(p)$ is the band structure (which requires $p \equiv hk/2\pi$) of the host material. Specification for the initial conditions $r(0)$ and $p(0)$ completes the input required by Eq. (1).

Despite its intimidating appearance, the Boltzmann equation has a straightforward physical interpretation: transport consists of a deterministic trajectory (a "free flight") obeying Eq. (2) which is randomly interrupted by scattering events determined by the W_α.[8] The scattering is assumed to be instantaneous and independent of both previous events and other electrons. Therefore, even apart from the approximation of semi-classical vs quantum dynamics, the Boltzmann equation is an approximate treatment of transport which is valid only in the limit of relatively infrequent scattering.[7][9] However, the validity of the Boltzmann equation has been asserted on theoretical grounds for electron transport in silicon subjected to fields as high as 10^7 V/cm.[10] Since the field in the SSPM is below 10^6 V/cm, it is expected that the Boltzmann equation is a valid description of transport in the SSPM.

The physical interpretation of the Boltzmann equation suggests the following random-walk algorithm:[8][11]

1. Select a random time interval τ.
2. Generate a deterministic electron trajectory from Eq. (2) over τ.
3. At the end of the trajectory, randomly select scattering mechanism α.
4. Reset the momentum according to $W_\alpha(p \rightarrow p')$.
5. Record the carrier position and momentum.
6. Go to Step 1 and repeat until finished.

The random time interval τ in Step 1 is selected from the exponential distribution $\exp(-\tau/\tau^0)/\tau^0$. The smallest available time step τ^0 is in turn taken to be the inverse of the maximum total scattering rate λ, where

$$\lambda(\rho) = \left(\frac{V_o}{8\pi^3}\right) \int dp' \sum_\alpha W_\alpha(p \rightarrow p'). \qquad (3)$$

Step 2 requires only the solution Eq. (2), for which a simple finite-difference scheme is employed. Figure 1 depicts a typical external electric field profile for the SSPM. Selection of the scattering mechanism α in step 3 is made by first weighting the mechanisms according to their individual scattering rates, $\lambda_\alpha = (V_o/8\pi^3) \int dp' W_\alpha(p \rightarrow p')$, and then choosing randomly among them. Of course, if no scattering mechanism were chosen, Step 4 would be skipped. For the single electron case, the simulation terminates with the first occurrence of impact-ionization, at which time its properties are recorded, and the algorithm is restarted

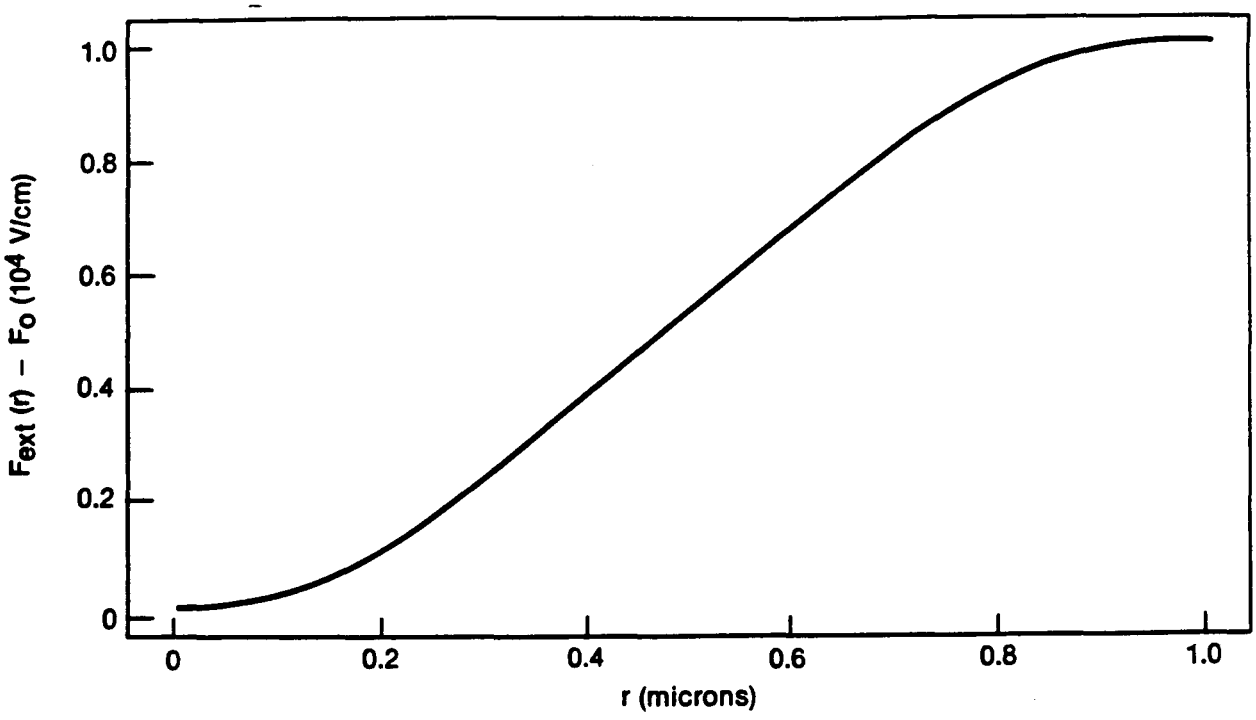

Figure 1. Model external electric field $F_{ext}(r) - F_o$ applied in the <100> direction. $F_o = 10^3$ V/cm. The position r is scaled by the length of the model cell. The gain region is from r = 0.05 to r = 0.9, about 4 microns.

until a statistically significant collection of trajectories is generated. In the multi-electron case, impact-ionization would produce a secondary electron; the respective trajectories of the primary, secondary, et seq electrons would then develop simultaneously. The simulation would continue until all the electrons had passed through the gain region and into the impurity-free blocking region of the SSPM.

The importance of the scattering mechanisms is apparent from the discussion of the algorithm. A thorough study of these mechanisms has begun and is briefly reviewed here. Only the scattering mechanisms due respectively to lattice phonons and neutral impurities need to be considered for the SSPM. The former are accurately characterized by semi-empirical formulae found in the literature,[12] but the latter are poorly understood. Electron scattering rates for phonon and impurity scattering are shown in Figure 2. Each of the scattering rates is sensitive to the temperature, density, dielectric constant, sound speed, and band structure of the host material. Throughout this report, only electrons in the conduction band of arsenic-doped silicon are considered, although the modifications required to accommodate other carriers or other materials are straightforward.

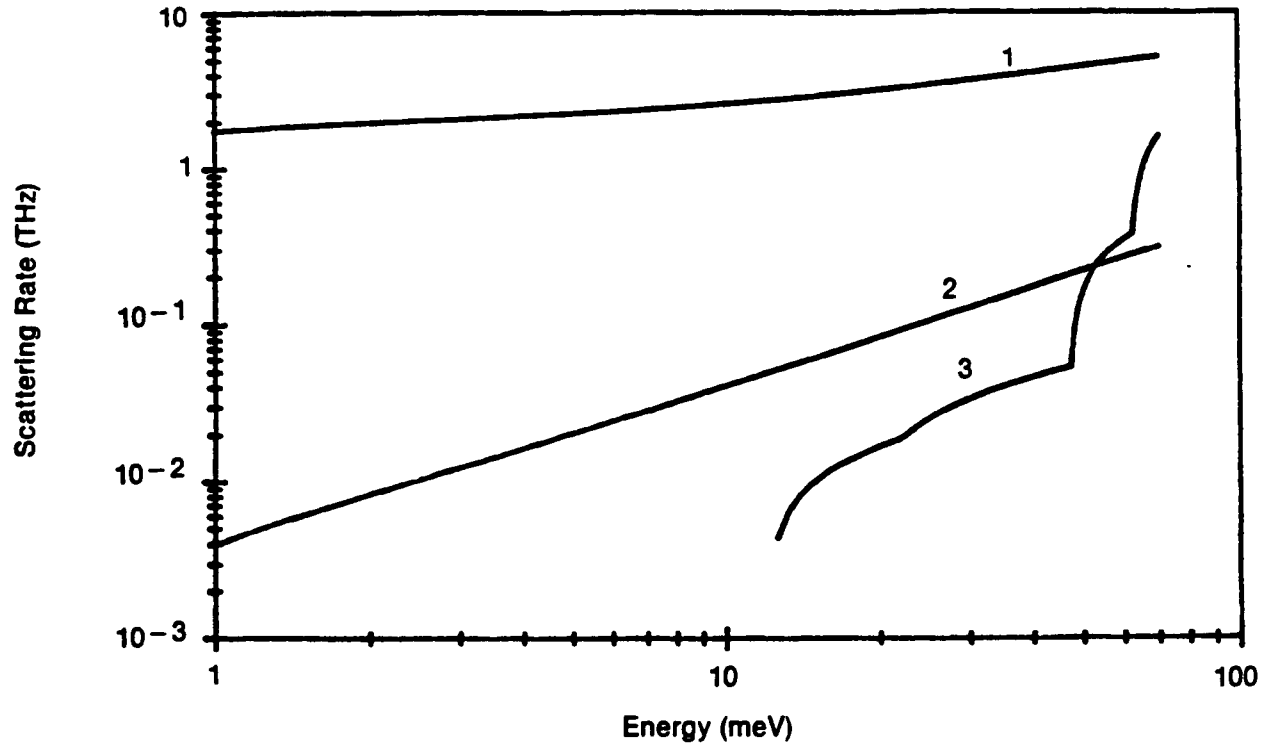

Figure 2. Electron scattering rates in silicon at 10K vs electron energy. Curve 1 is for neutral impurity scattering. [15] Curve 2 is for acoustic intervalley scattering. [10] Curve 3 is the maximal intervalley scattering rate. [10]

In present versions of the SSPM, only phonon emission can contribute significantly to the scattering of electrons by phonons.[13] The scattering mechanisms due to phonons considered here are, respectively, acoustic phonon intravalley scattering, acoustic intervalley scattering, and optical intervalley scattering. There are three separate mechanisms for each of the latter two kinds of scattering, according to which of the six valleys of the silicon conduction band is involved in the electron scattering. Figure 2 shows that below the ionization threshold of 45 meV for arsenic-doped silicon, there is little contribution to $\lambda(p)$ from intervalley scattering. Therefore, intravalley scattering requires careful treatment. The usual approximation that intravalley scattering is elastic and isotropic is inappropriate, as Figures 3 and 4 show. Figure 3 depicts the distribution of scattered electron energy, and shows that the energy loss is appreciable, if not overwhelming. Figure 4 depicts the distribution of the angle theta between the incoming and outgoing momentum, and shows that the angles are clustered about 90°, rather than uniformly distributed.

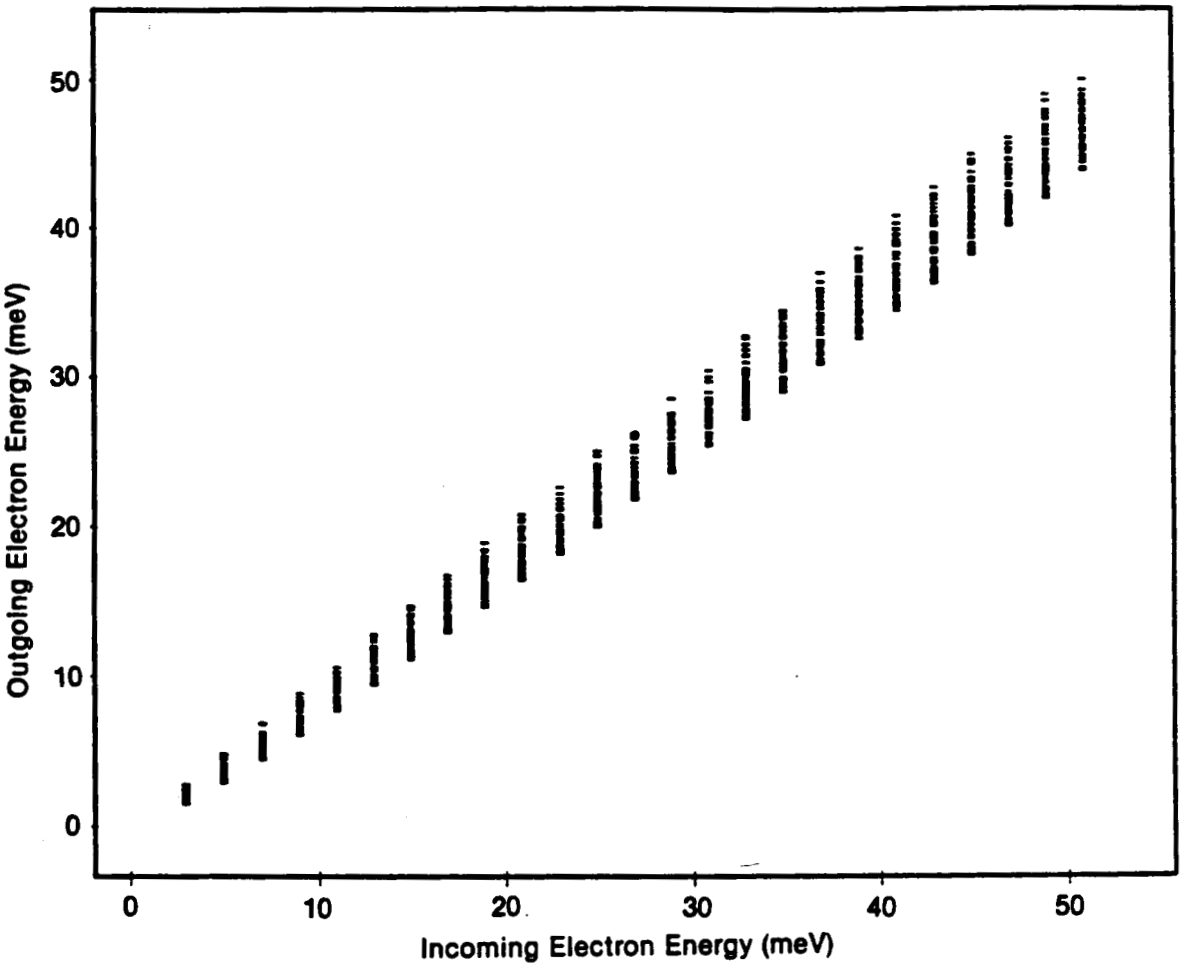

Figure 3. Acoustic-phonon scattering energy distribution (T = 7K) for 25 energies with 100 samples each.

The most important scattering mechanisms due to impurities are neutral-impurity scattering and neutral-impurity impact-ionization. Impact ionization is central to the operation of the SSPM, for it generates the secondary electrons which constitute the avalanche. Although an isolated arsenic impurity in silicon has an ionization potential of 54 meV, arsenic impurities in the SSPM may be ionized by electrons with energy as low as 45 meV.[14] The treatment of neutral-impurity impact ionization (as distinguished from the more carefully studied band-to-band impact ionization) has been crude, and rests primarily on analogies to impact ionization of atomic hydrogen by energetic electrons.[15] However, it is difficult to assess experimentally the sensitivity of electron dynamics and development of the avalanche to details of the scattering rate; it may happen that a more-detailed treatment is not warranted. Impact-ionization in the single-electron simulation terminates the trajectory.

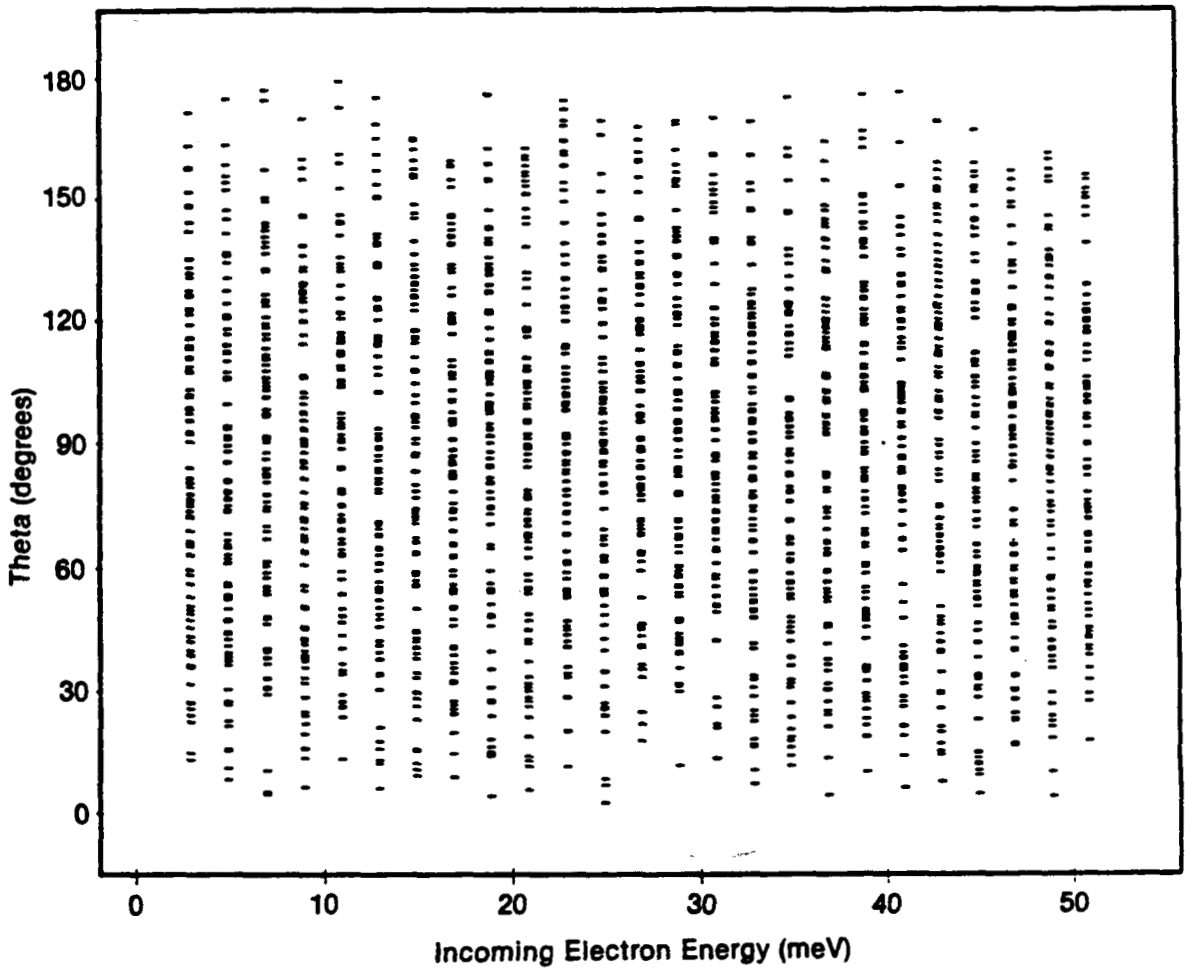

Figure 4. Acoustic-phonon scattering angle distribution (T = 7K) for 25 energies with 100 samples each.

Neutral-impurity scattering is inaccurately treated by current theories, and experimental data is incomplete. Although the present implementation of the SSPM electron transport model employs current neutral-impurity scattering theory, improvements should be investigated along the lines discussed below, since the results may be more sensitive to the details of this kind of scattering than for impact-ionization. The only channels of energy dissipation currently considered in SSPM theory are impact ionization and phonon scattering. Of these, only acoustic phonon scattering dissipates strongly below the ionization threshold. Because achievement by the electron of the threshold energy for impact ionization is central to the operation of the SSPM, it may be necessary to consider other sub-threshold dissipative channels. In present theories, neutral impurity scattering (e-N) is treated elastically; further, the scattering rate is both isotropic and energy-independent. This treatment of e-N scattering

is based on early calculations for the cross section of electron-Hydrogen (e-H) scattering.[16][17] The resulting scattering rates are inaccurate in all but a narrow energy regime. Subsequent attempts to modify this treatment have been few and disappointing.[18] In contrast to these earlier treatments, the following reflect the current status of e-H scattering:

1. Accurate data and computations are available.[19]

2. The scattering may be strongly energy dependent, especially near the ionization threshold.

3. The collisions may be either elastic or strongly inelastic, depending on the incident electron energy.

4. The scattering rate is strongly anisotropic for all but a narrow energy range.

Since neutral impurity scattering may become strongly inelastic at sub-threshold energies, it may be an important or even dominant source of sub-threshold dissipation. Two independent alternatives to improve the e-N scattering model being considered are:

1. Rescale the known e-H results to those for a donor impurity in silicon. (However, this requires an effective mass approximation which may not be appropriate for silicon).

2. Accurate variational Green functions calculations for e-H scattering became available in the mid-1970's;[19] more recently, accurate semi-empirical wave-functions for shallow donors in silicon were published.[20] Substitution of these wave-functions in the variational Green function scattering calculation should produce accurate scattering cross sections.

In the multi-electron simulation of the avalanche, other scattering mechanisms may be required. Electron-electron scattering may be important if the electron density becomes sufficiently high in the gain-region. Ionized impurity scattering and recombination events, a form of scattering, may also be required if the density of ionized impurities becomes high. These considerations have been deferred for the present and will be examined in future work.

3.3 COMPUTATIONS

Current efforts are devoted to producing accurate single-carrier solutions of the Boltzmann equation computed by the random-walk techniques discussed above. Figure 5 shows the kinetic energy of a single electron for a single trajectory in a simple model for the SSPM, where the gain region is 4 μm long along the <100> axis. The electric field is applied along the <100> axis, with the profile shown in Figure 1. Impact-ionization has been omitted; only

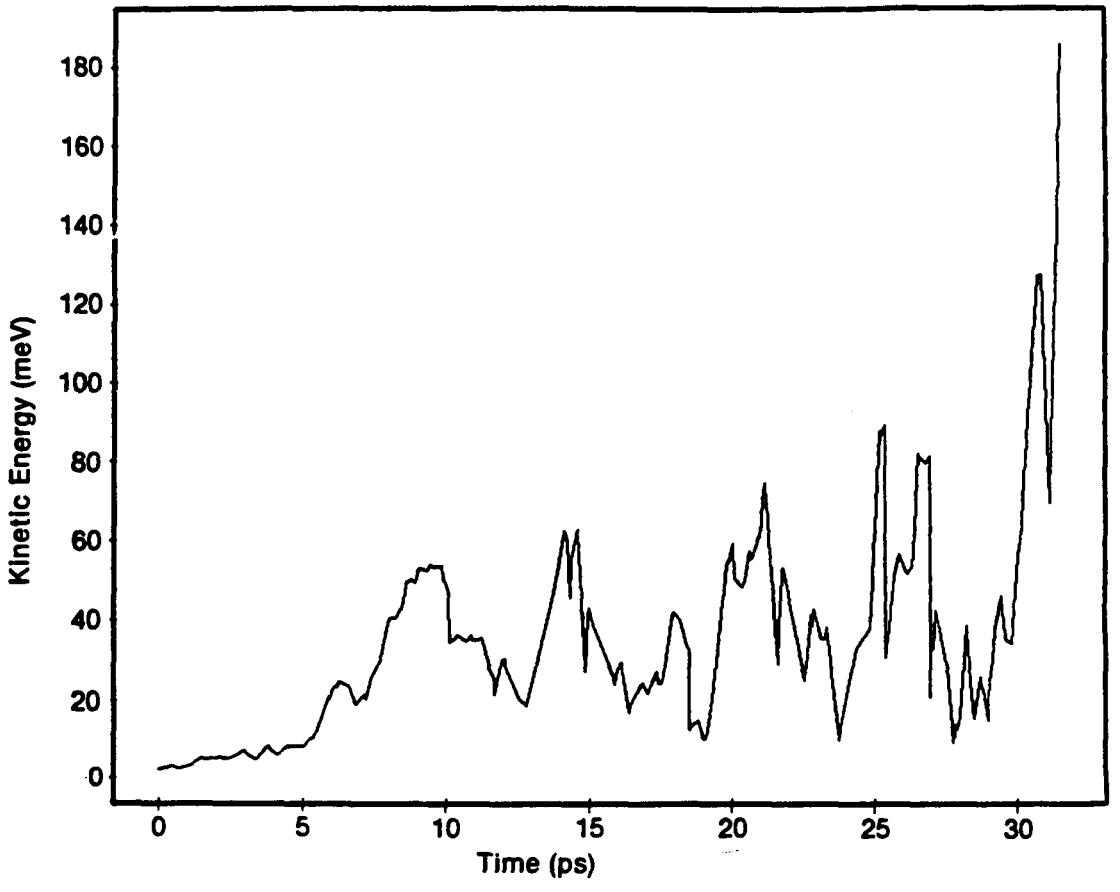

Figure 5. Energy evolution of a single electron in a model SSPM.

phonon and neutral-impurity (elastic and isotropic) scattering have been included. The sharpest decreases in energy are due to phonon emission; other decreases are accounted for by electron scattering against the field. The first opportunity for impact-ionization for this trajectory occurs about 10 ps after the electron's entry into the gain region. As Figure 6 shows, this corresponds to a distance of about 0.8 μm into the gain region. The omission of impact-ionization leads to unrealistic and uncontrollable accelerations as the electron reaches the center of the gain region.

The computations can be performed most effectively on the vector XMP at the Ames Computational Facility. The XMP allows vector operations which occur throughout the code (e.g., the dot product, matrix operations) to be performed nearly as fast as if they were scalar operations. The resulting gain in speed can be more than a factor of ten over equivalent machines employing only scalar operations. However, the programs must often be coded in special ways to take advantage of vectorization, and therefore some effort has been devoted to optimization of the code.

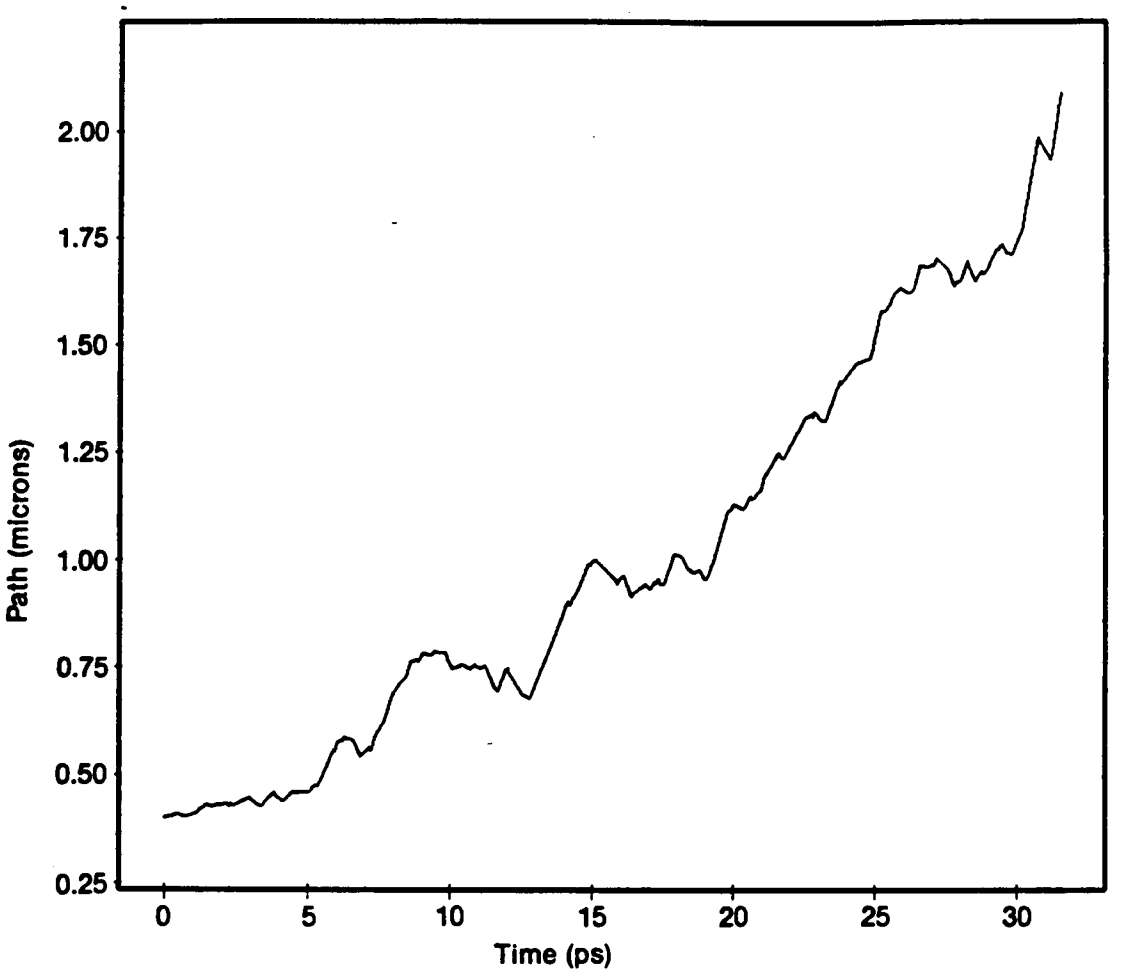

Figure 6. Path evolution of a single electron in a model SSPM. The path is the <100> projection of the trajectory.

The computations require not only a fast computer with substantial core memory but also a network to transfer large data files between Rockwell and the computer. A network (through the Jet Propulsion Lab to the ARC XMP) planned for the first quarter of 1988 did not become operational until the end of June 1988. Therefore, the extensive computations planned on the Ames XMP have not been carried out in time for this report. The network is especially important for the kind of problem pursued here because of the frequent interaction anticipated between the output and subsequent modifications to the programs. In contrast, other kinds of computations which have been pursued on the Ames XMP could be run nearly automatically, thereby reducing the need to have ready access to the output. While a small dedicated vector-processor has been acquired by Rockwell, its anticipated speed has yet to be realized. Therefore, continued reliance upon the ARC XMP and its network is anticipated in order to complete these computations.

3.4 APPLICATIONS TO NASA REQUIREMENTS

NASA's requirement for high SSPM quantum efficiency involves, among other considerations, high gain and narrow gain-dispersion. The single-electron microscopic transport calculation immediately yields the parameters required by the phenomenological theory of electron avalanche development in the SSPM.[14] That theory in turn yields the gain, gain dispersion, and any combination of moments for the electron pulse-height distribution. For a given material, modification in the SSPM configuration changes the external electric field, which appears explicitly in the Boltzmann equation (Eqs. 1 and 2). The temperature also appears explicitly in the scattering rates. Therefore, changes in design or operating temperature can be incorporated explicitly into the theory. Another NASA requirement calls for the investigation of alternate materials for the SSPM. Again, changes in the materials can be incorporated explicitly by the transport theory through modifications to the band structure, scattering rates and electric field.

The combination of single-electron transport simulation and phenomenological theory provides an economical alternative to the direct simulation of avalanches generating over 50,000 electrons. However, in order to respond to the NASA goals for elucidation and control of the SSPM dynamic response, the direct simulation is required, and therefore is planned for future work.

3.5 TASK ASSESSMENT

The microscopic single-electron transport theory for the SSPM is ready to be implemented for large-scale computations. The gain and gain dispersion of the SSPM will be among the first parameters to be calculated. Computational requirements which include an operating network to NASA-Ames computers will probably be met by July 1988, thereby expediting future work which will consist of the multi-electron simulation of the SSPM and improvement of the neutral-impurity scattering theory.

4.0 SSPM FABRICATION AND CHARACTERIZATION

4.1 INTRODUCTION

A process lot of SSPM wafers was fabricated as part of the work on this phase of the program. Results of experimental and theoretical work undertaken to fabricate, characterize and understand SSPMs for use in astronomy applications are presented and discussed in this portion of the report. Section 4.2 covers materials growth, materials characterization and device fabrication. Section 4.3 presents device characterization data, analysis of measurements performed on the fabricated detectors, and equations to describe the results.

Figure 7 shows the experimental setup used to measure SSPM characteristics, and Figure 8 displays typical electronics used in making the measurements.

4.2 SSPM FABRICATION

4.2.1 Materials Growth and Characterization

The SSPMs described in this report were fabricated by growing doped and undoped silicon epitaxial layers, using a chemical vapor deposition (CVD) process, on silicon substrates. The wafers were then patterned into detectors using established microfabrication techniques.

Epitaxial layer doping levels and thicknesses (Figure 9) are the most important factors in determining the performance of a SSPM. In order to measure the acceptor (boron) levels (N_A) and verify that they were being obtained even in the presence of donor (arsenic) concentrations (N_D) about 10^4 times higher, a cryogenic capacitance-versus-voltage (CV) technique has been developed and is being utilized for wafer acceptance screening.[21] The reactor was calibrated using CV data gathered from CVD test wafers prior to growing the actual detector wafers' infrared-active layers.

Data comparing N_A in high- and low-performance devices are shown in Figure 10. The higher level of N_A ($>10^{14}$ atoms/cm^3) shown in the right-hand plot is responsible for the poor device performance. The rate of change of electric field strength with depth is proportional to N_A in this doping range. So, if N_A is too high, the field drops too quickly, resulting in a thin gain region at high biases. This was the cause of the low gain and high bias currents obtained from the low-performance device sample. At the other extreme, a low N_A would cause the gain region to be very thick, resulting in excessive gain dispersion.

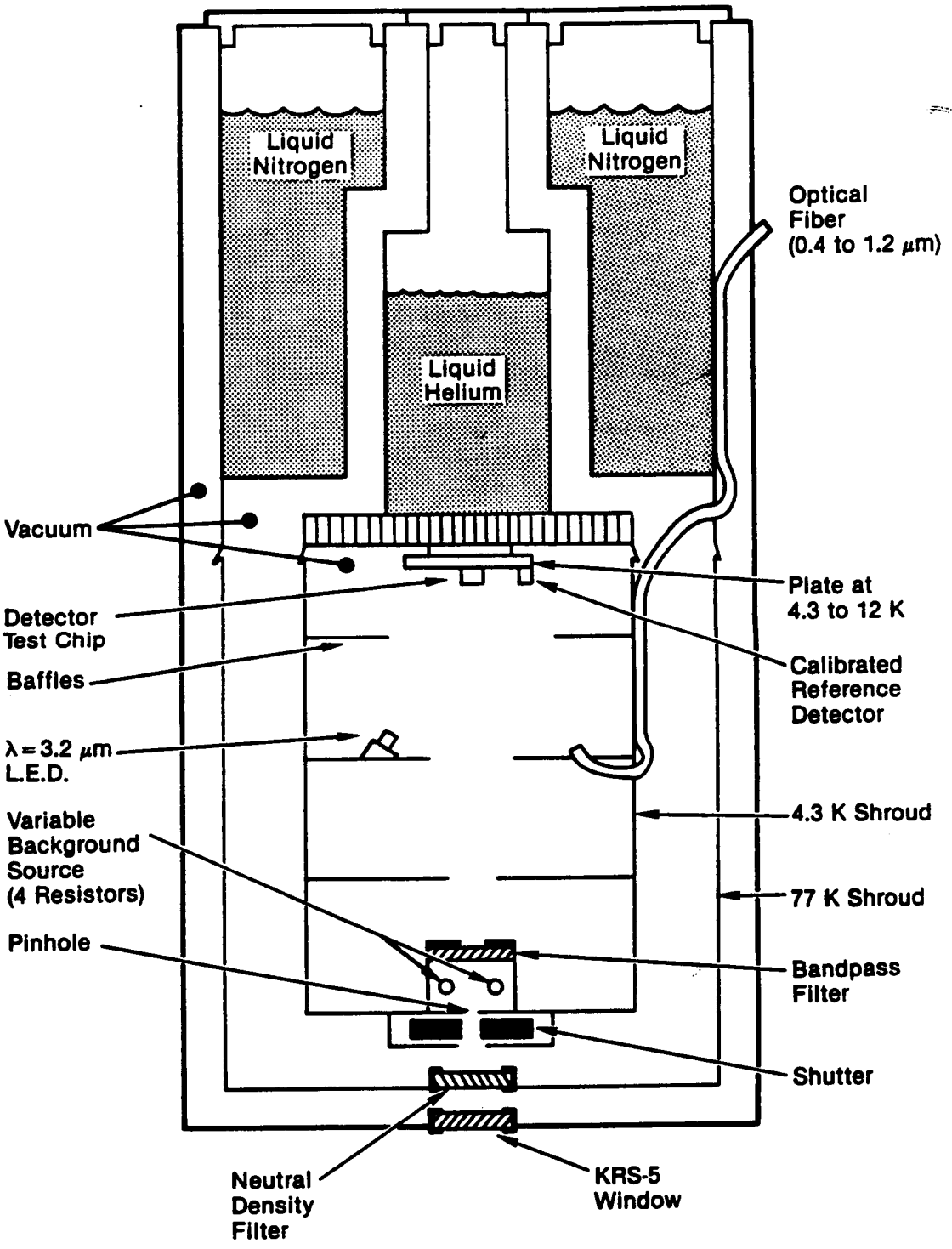

Figure 7. Experimental setup for measurement of SSPM parameters

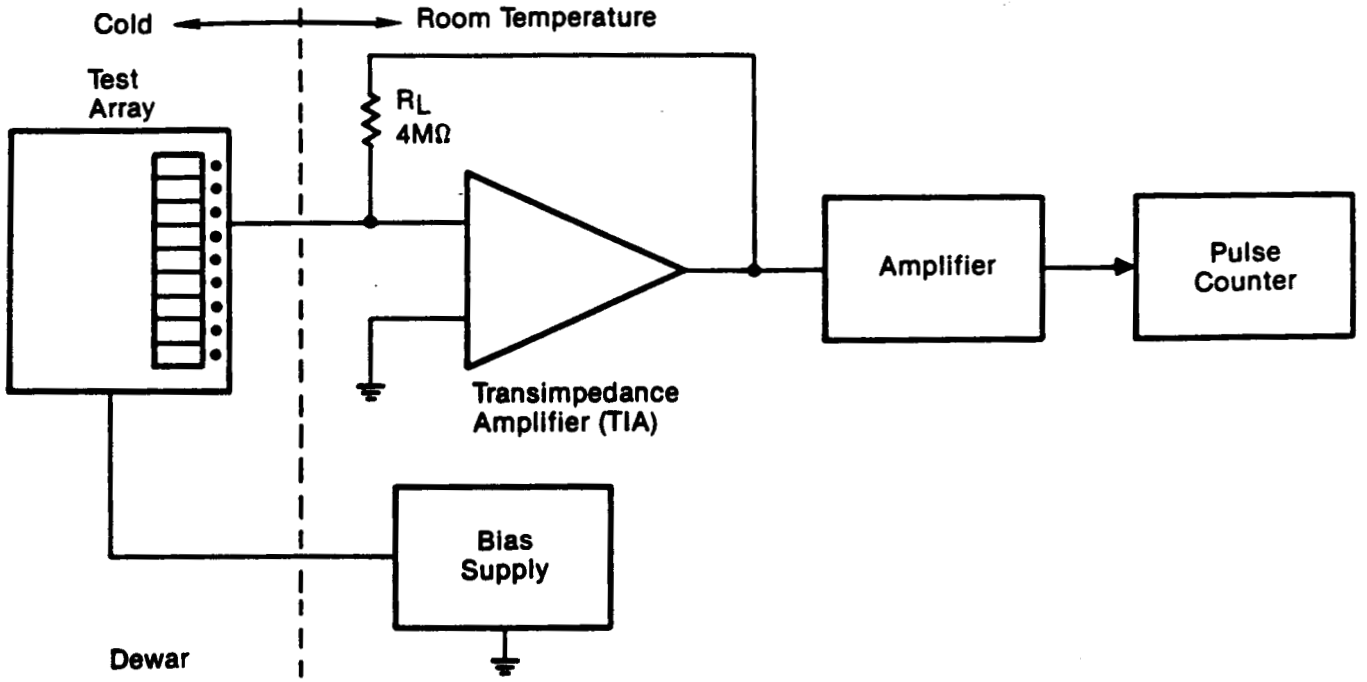

Figure 8. Typical electronics for SSPM testing

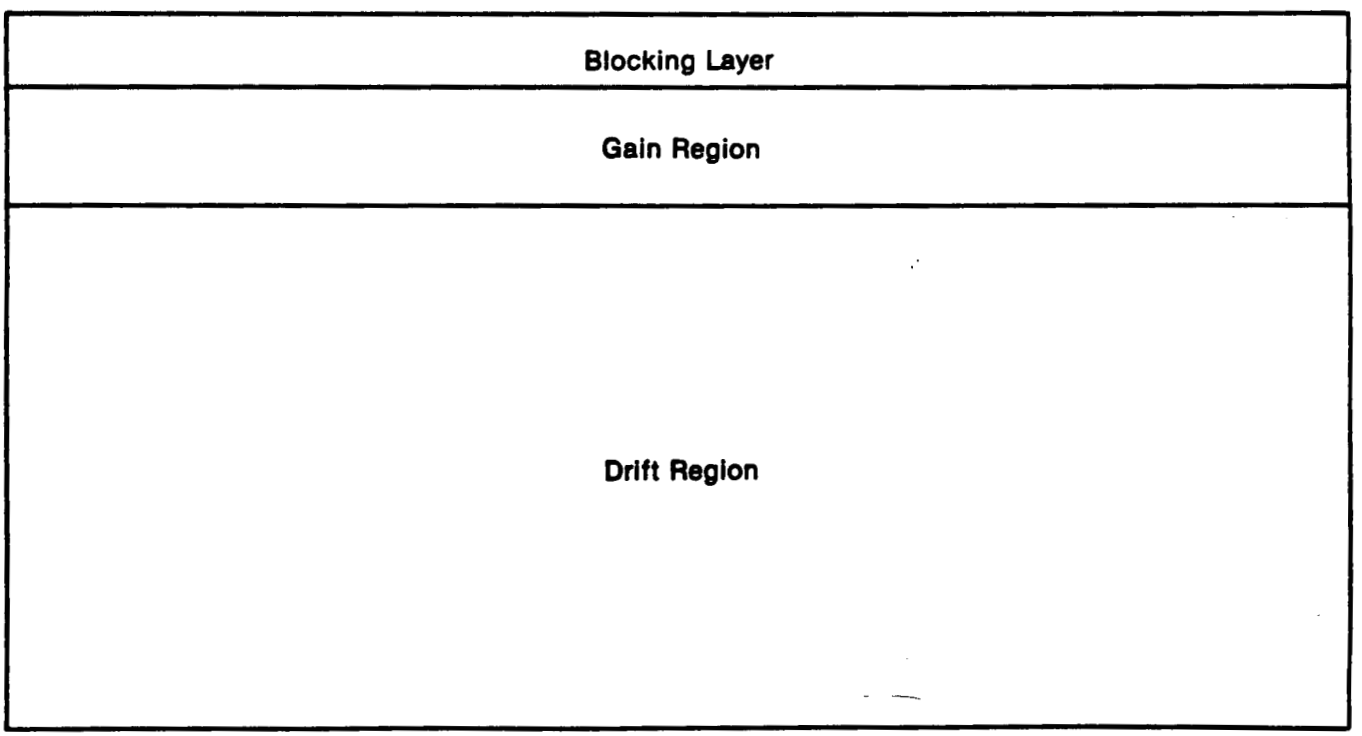

Figure 9. Schematic diagram of SSPM epitaxial layers

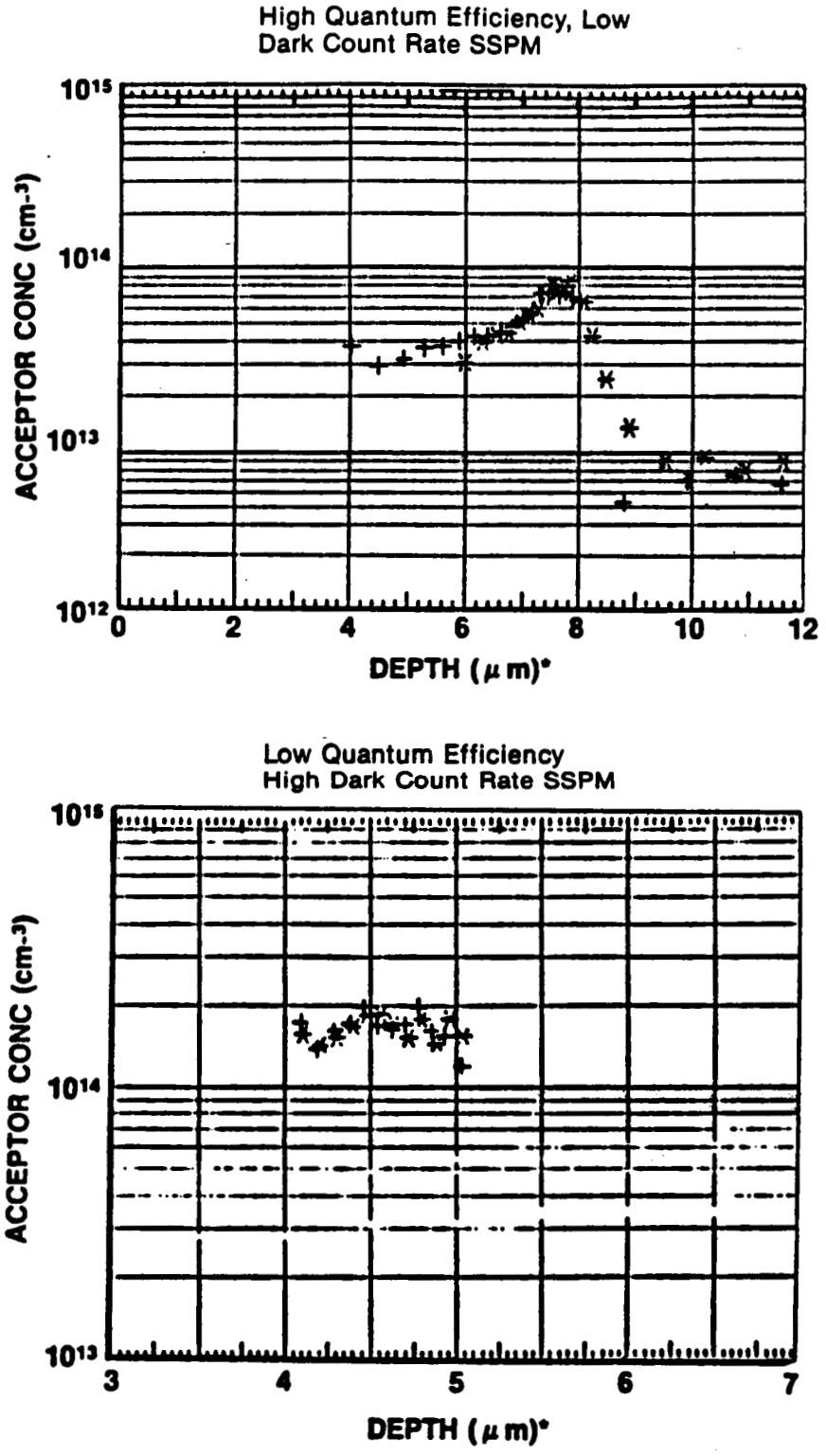

Figure 10. Comparison of acceptor profiles in material producing good and poor devices (CV data).

Three different groups of epitaxial layers are represented by the fabricated detectors. The target doping levels, as well as the acceptor levels actually measured using CV analysis of detector wafers, are shown in Table II. The differences between the target and actual values of N_A, and N_D and thickness were within the experimental uncertainties of the techniques used to measure these quantities. It was anticipated, based on past experience, that the Group 1 devices would have higher gain and lower gain dispersion than the Group 2 or Group 3 SSPMs. The tradeoff was that the absence of intentionally introduced acceptors in the drift regions of the Group 2 and Group 3 detectors might result in higher counting quantum efficiencies.

After detectors were fabricated using these wafers (see Section 4.2.2), three 32 x 32 mil^2 SSPMs from each of the three groups in the lot were packaged and acceptor profiles in their infrared-active regions were measured using the CV technique. These measurements verified that the desired acceptor concentrations and profiles were present in the finished devices. The results are shown in Figure 11, where it can be seen that the differences in N_A are relatively small. The fact that devices from these groups showed significant

Table II. Doping profiles of epitaxial material for device fabrication

	Blocking Layer	Gain Region			Drift Region	
Growth Runs	Thickness (μm)	Thickness (μm)	N_D* (atoms /cm^3)	N_A (atoms /cm^3)	Thickness (μm)	N_D (atoms /cm^3)
GROUP 1						
target:	3.5	27	5.5×10^{17}	5.0×10^{13}	(included with gain region)	
actual:	3.5	27	5.5×10^{17}	5.6×10^{13}		
GROUP 2						
target:	3.5	6	5.5×10^{17}	5.0×10^{13}	25	5.5×10^{17}
actual:	3.5	5.5	4.9×10^{17}	5.2×10^{13}	25	4.9×10^{17}
GROUP 3						
target:	3.5	5	5.5×10^{17}	6.0×10^{13}	25	5.5×10^{17}
actual:	3.5	5	5.3×10^{17}	6.3×10^{13}	25	5.5×10^{17}

*Donor concentrations were measured using spreading resistance profiling (SRP)

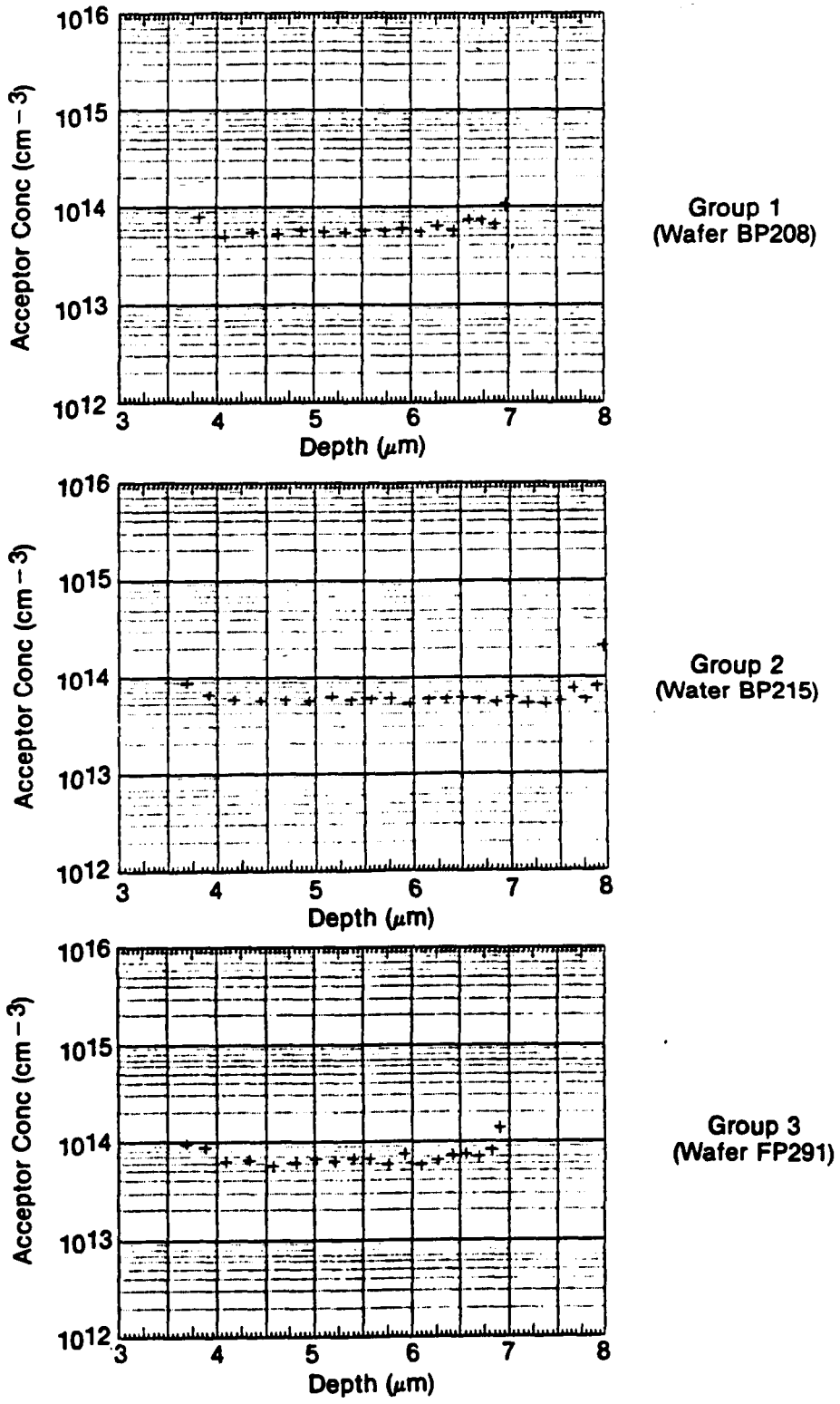

Figure 11. Acceptor profiles from each epitaxy group

performance differences indicates that device operation is highly sensitive to the N_A profile in the SSPM's gain region. This sensitivity results from the exponential dependence of impact ionization probability on electric field strength, coupled with the linear dependence of the rate-of-change of electric field strength on acceptor concentration.

Note that the CV technique did not profile the entire infrared-active layer. This is because the resistive part of the AC signal eventually dominated the capacitive part as the DC detector bias was increased during the measurements. When this condition occurs, the the finite phase stability of the lock-in amplifier caused confusion between the resistive and capacitive parts of the signal and the technique was no longer operable.

4.2.2 Detector Fabrication

Three wafers from each of the three epitaxy groups were selected for processing into detectors, and two of these nine wafers broke during processing. Partial characteristics of the seven wafers that completed processing are summarized in Table III. The first letter in the wafer identification denotes whether the devices are suitable for front- (F) or back-illumination (B). The front-illuminated samples were grown on doped substrates which are opaque to the wavelengths of interest. The opacity is useful for reducing optical crosstalk between front-illuminated array pixels.

Table III. Finished SSPM Wafers from Lot PM-79

Wafer	Substrate Type*	Epitaxy Group No.
BP225	intrinsic	1
FP293	extrinsic	1
BP231	intrinsic	2
BP232	intrinsic	2
BP233	intrinsic	3
BP234	intrinsic	3
FP296	extrinsic	3

*The extrinsic substrates were doped to above the metal-insulator transition with an n-type dopant (antimony).

Detector geometries were defined using the mask set which had been developed on Rockwell IR&D. Each finished SSPM wafer contained 36 copies of the die in a 6 x 6 pattern. Some corner dice ran slightly past the edges of the wafers and were therefore incomplete. A diagram of the die and a brief description of each of the structures is shown in Figure 12.

4.3 SSPM CHARACTERIZATION

4.3.1 Quantum Efficiency and Dark Count Rate

The quantum efficiencies and dark count rates of SSPMs mounted for back-illumination were measured as functions of temperature and bias voltage at wavelengths of 3.2 and 20 μm. The dark count rates were measured at backgrounds less than 5×10^6 photons/cm^2-s. Due to a recently-uncovered problem with the low-background calibration of standard detectors (photo-conductors) that were to be used as references, the incident flux levels were measured using SSPMs from lots discussed in a previous report.[3] Data gathered on other programs indicated that the standard SSPM from Lot PM-63 (see Section 5.0 of Ref. 4) had a quantum efficiency η of about 45% at T = 7 K, V_{bias} = 7.7 V, and λ = 20 μm. However, this value has not yet been checked directly against a well-characterized secondary standard detector.

Detectors from each of the three groups were characterized. Data from a representative back-illuminated 200 x 200 μm^2 SSPM from each group were obtained, and are shown in Tables IV and V and plotted in Figures 13, 14, and 15. The data show that SSPMs from the second group have the highest maximum quantum efficiencies, while maintaining low dark count rates and bias currents. All three epitaxy groups show much lower dark count rates than any previous SSPMs at the same temperature.

The quantum efficiencies plotted in Figures 13, 14 and 15 were calculated from the data using

$$\eta = (f_{illum} - f_{dark})/(\Phi A).$$

where f_{illum} is the count rate measured with an incident flux Φ, f_{dark} is the dark count rate and A is the SSPM area.

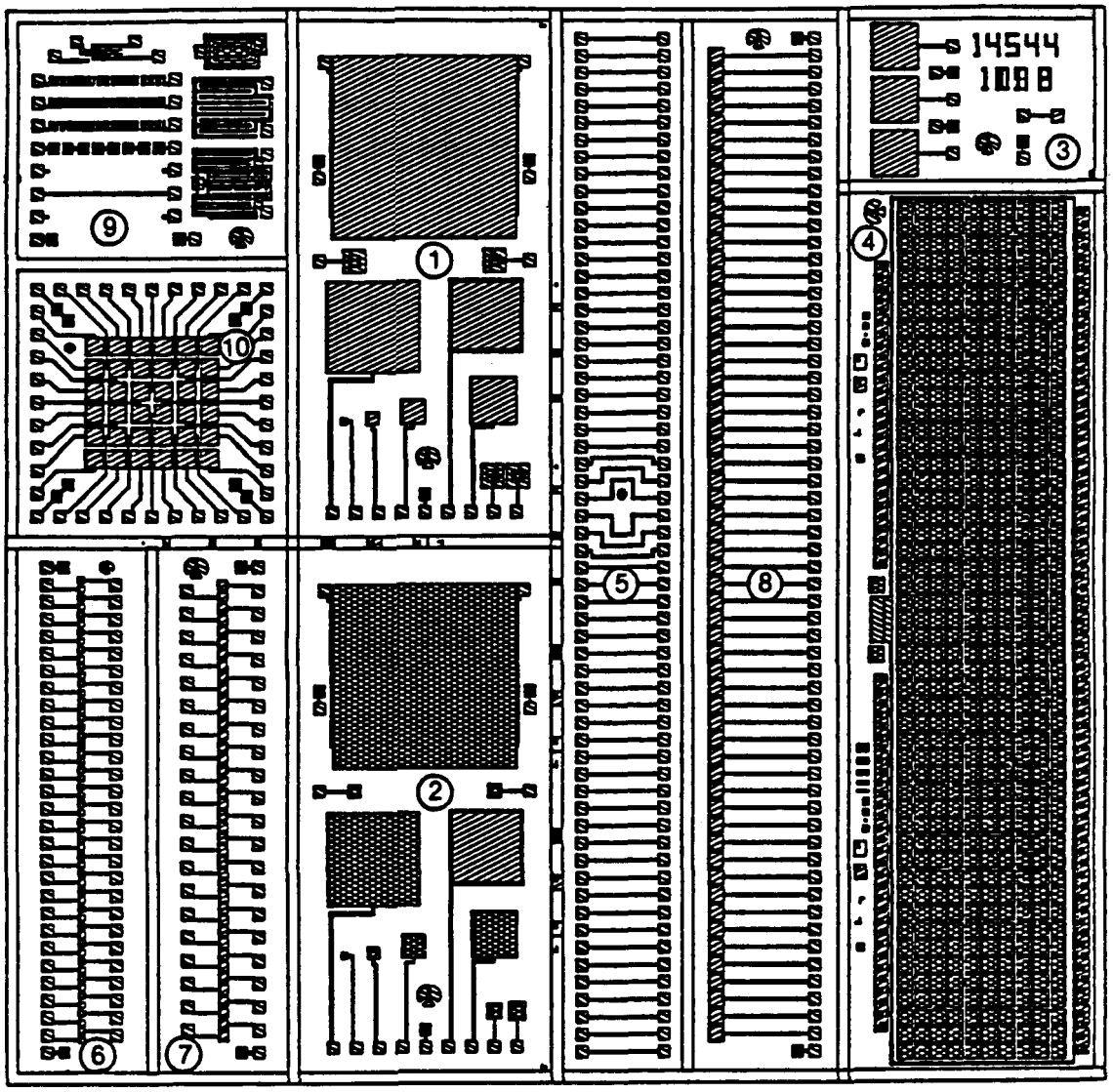

1. Set of Front-Illuminated Detectors of Different Area (2×2 to 64×64 m)
2. Set of Back-Illuminated Detectors of Different Area (2×2 to 64×64 m)
3. 20×20 mil Block of 3 Detectors
4. 10×50 Area Array (5×5 mil)
5. Set of Metalization and Pads for Connecting Front-Illuminated Line Array to Multiplexer
6. 7. 8. Line Arrays: 2×2, 3×3, 5×5 mil
9. Various Test Devices
10. Front-Illuminated 6×6 Array of 6×6 mil Detectors

Figure 12. SSPM Die Layout

Table IV. Count Rates (counts/s) of SSPM pixels from Each Group at λ = 3.2 μm. $\Phi_{illum} = 1.7 \times 10^6$ ph/cm^2-s, $\Phi_{dark} < 5 \times 10^6$ ph/cm^2-s

Bias (V)	Temp (K)	Epitaxy Group: Group 1 Illum	Group 1 Dark	Group 2 Illum	Group 2 Dark	Group 3 Illum	Group 3 Dark
6.0	6	0	0	*	*	*	*
6.2	6	4	0	*	*	*	*
6.4	6	5	0	*	*	6	6
6.6	6	18	2	*	*	9	7
6.8	6	65	7	*	*	15	10
7.0	6	-	-	23	1	49	15
7.2	6	-	-	78	6	117	26
7.4	6	-	-	215	28	258	50
7.6	6	-	-	444	58	445	95
6.0	7	3	1	0	0	1	0
6.2	7	5	0	0	0	0	0
6.4	7	36	0	0	0	5	5
6.6	7	112	3	5	0	15	5
6.8	7	241	12	46	0	61	13
7.0	7	-	-	128	6	156	30
7.2	7	-	-	299	43	357	76
7.4	7	-	-	597	75	651	150
7.6	7	-	-	-	-	-	-
6.0	8	40	3	4	1	0	0
6.2	8	101	7	13	1	5	0
6.4	8	230	20	39	4	23	4
6.6	8	420	50	108	12	93	14
6.8	8	-	-	260	22	265	51
7.0	8	-	-	517	52	615	133
7.2	8	-	-	915	93	1108	278
7.4	8	-	-	-	-	-	-
6.0	9	145	18	20	0	9	0
6.2	9	300	52	75	4	43	6
6.4	9	563	127	185	13	136	19
6.6	9	936	268	411	45	356	58
6.8	9	-	-	743	80	763	165
7.0	9	-	-	1234	152	1392	363
7.2	9	-	-	1812	239	2272	705
7.4	9	-	-	-	-	-	-

Table IV. (Continued)

Bias (V)	Temp (K)	Epitaxy Group: Group 1 Illum	Group 1 Dark	Group 2 Illum	Group 2 Dark	Group 3 Illum	Group 3 Dark
6.0	10	544	358	77	4	26	4
6.2	10	1257	947	192	29	81	20
6.4	10	2657	2171	432	66	241	53
6.6	10	5000	4375	833	173	579	166
6.8	10	-	-	1441	357	1195	412
7.0	10	-	-	2241	708	2104	890
7.2	10	-	-	3187	1322	-	-
7.4	10	-	-	-	-	-	-
6.0	11	3977	3842	250	150	35	17
6.2	11	8895	8755	681	471	133	82
6.4	11	+	+	1630	1266	466	277
6.6	11	+	+	3531	2954	1238	859
6.8	11	-	-	6637	5841	2868	2280
7.0	11	-	-	11342	10279	5555	4783
7.2	11	-	-	-	-	-	-

*Signal below noise
-After breakdown
+Limited by speed of measurement electronics

Table V. Count Rates (counts/s) of SSPM pixels from Each Group at λ = 20 μm. $\Phi_{illum} = 1.2 \times 10^{8}$ ph/cm^2-s, $\Phi_{dark} < 5 \times 10^{6}$ ph/cm^2-s

Bias (V)	Temp (K)	Epitaxy Group: Group 1 Illum	Group 1 Dark	Group 2 Illum	Group 2 Dark	Group 3 Illum	Group 3 Dark
6.0	6	0	0	*	*	*	*
6.2	6	1	0	*	*	*	*
6.4	6	9	0	*	*	6	6
6.6	6	41	2	*	*	10	7
6.8	6	161	7	*	*	22	10
7.0	6	-	-	53	1	70	15
7.2	6	-	-	191	6	207	26
7.4	6	-	-	487	28	489	50
7.6	6	-	-	975	58	1002	95
6.0	7	7	1	0	0	1	0
6.2	7	28	0	0	0	0	0

Table V. (Continued)

Bias (V)	Temp (K)	Epitaxy Group: Group 1 Illum	Group 1 Dark	Group 2 Illum	Group 2 Dark	Group 3 Illum	Group 3 Dark
6.4	7	103	0	2	0	5	5
6.6	7	289	3	25	0	26	5
6.8	7	700	12	127	0	102	13
7.0	7	-	-	390	6	301	30
7.2	7	-	-	874	43	700	76
7.4	7	-	-	1645	75	1326	150
7.6	7	-	-	-	-	-	-
6.0	8	77	3	5	1	0	0
6.2	8	227	7	24	1	9	0
6.4	8	536	20	99	4	54	4
6.6	8	1076	50	317	12	205	14
6.8	8	-	-	788	22	561	51
7.0	8	-	-	1553	52	1196	133
7.2	8	-	-	2686	93	2137	278
7.4	8	-	-	-	-	-	-
6.0	9	270	18	54	0	23	0
6.2	9	648	52	196	4	105	6
6.4	9	1257	127	574	13	333	19
6.6	9	2213	268	1288	45	851	58
6.8	9	-	-	2424	80	1783	165
7.0	9	-	-	3953	152	2999	363
7.2	9	-	-	5818	239	4692	705
7.4	9	-	-	-	-	-	-
6.0	10	738	358	181	4	52	4
6.2	10	1719	947	546	29	201	20
6.4	10	3495	2171	1302	66	596	53
6.6	10	6296	4375	2599	173	1415	166
6.8	10	-	-	4344	357	2776	412
7.0	10	-	-	6496	708	4717	890
7.2	10	-	-	8958	1322	-	-
7.4	10	-	-	-	-	-	-
6.0	11	4132	3842	402	150	70	17
6.2	11	9227	8755	1138	471	268	82
6.4	11	+	+	2655	1266	844	277
6.6	11	+	+	5344	2954	2126	859
6.8	11	+	+	9131	5841	4389	2280
7.0	11	+	+	14569	10279	7751	4783
7.2	11	+	-	-	-	-	-

*Signal below noise
-After breakdown
+Limited by speed of measurement electronics

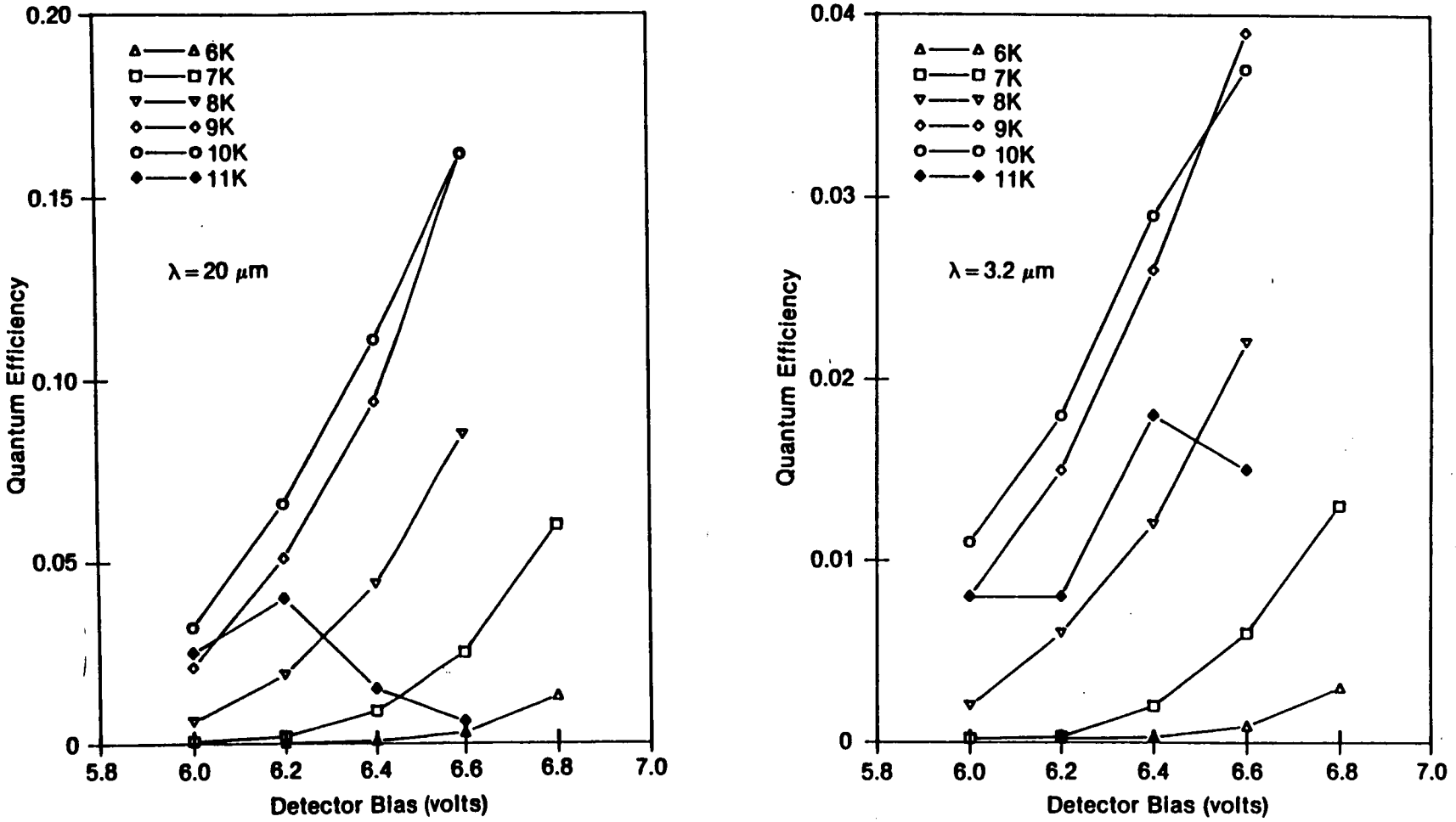

Figure 13. Quantum efficiency of group 1 SSPMs as a function of bias. Noisy data at 11 K is due to very high dark count rates.

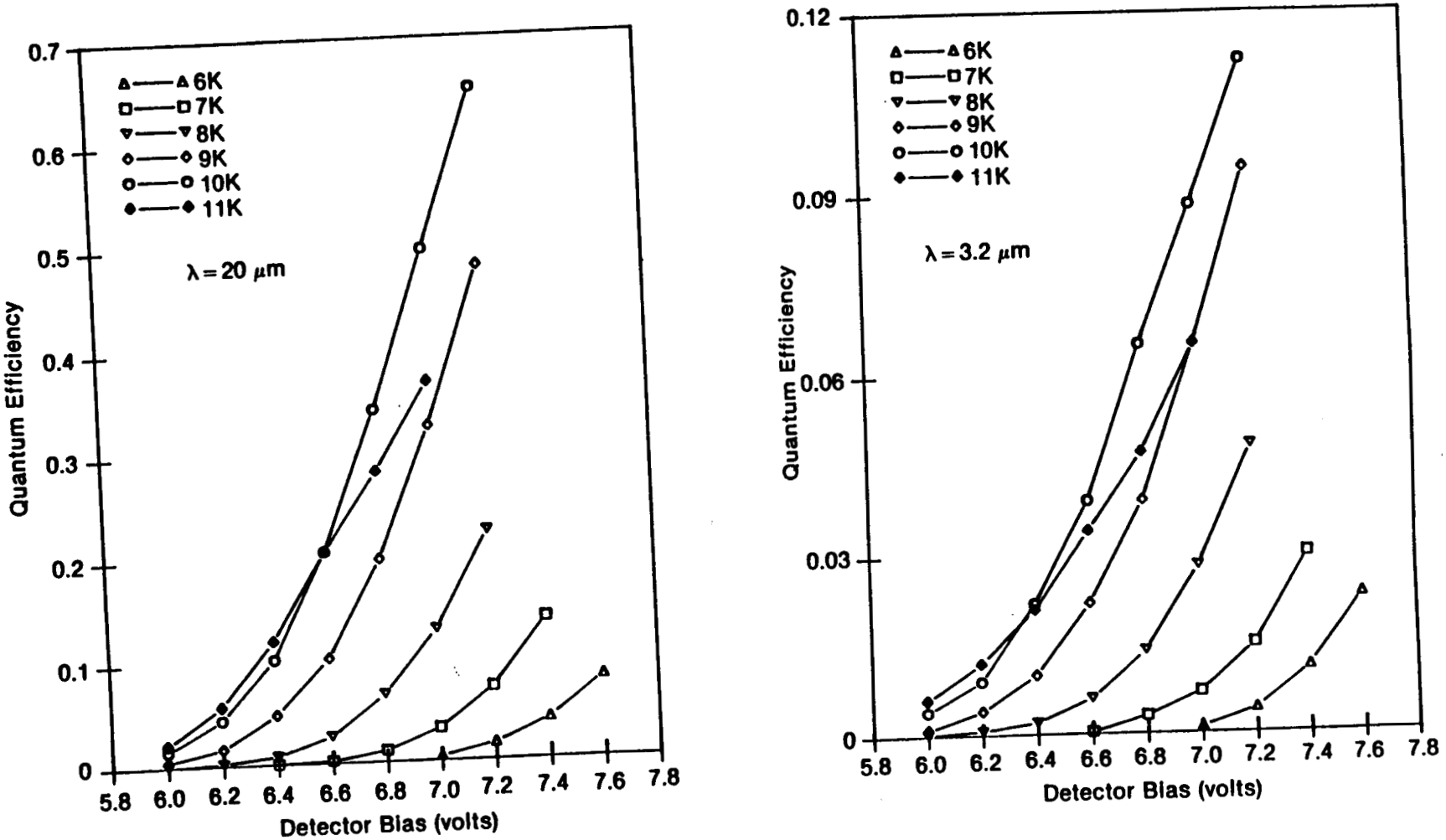

Figure 14. Quantum efficiency of Group 2 SSPMs as a function of bias.

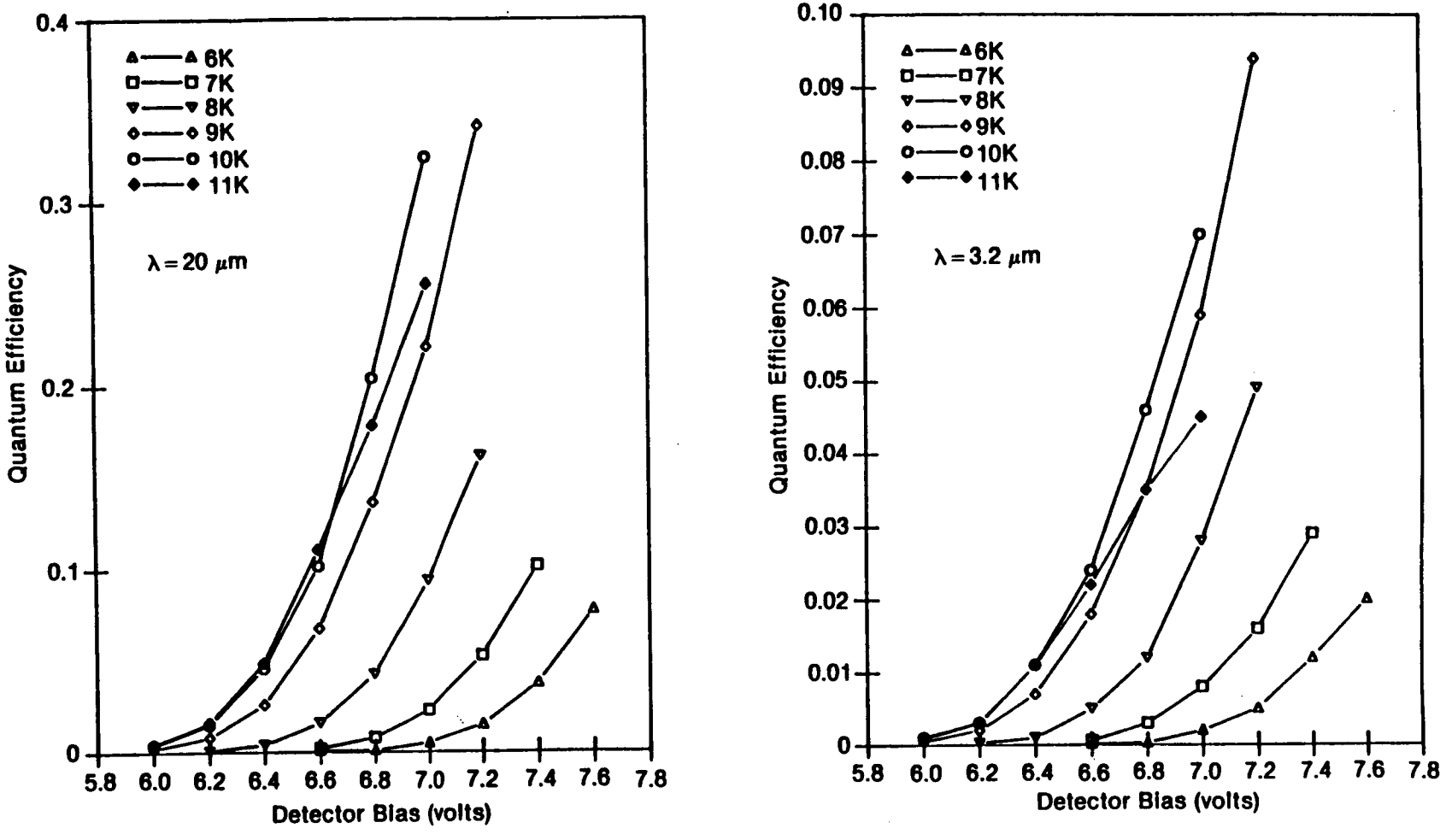

Figure 15. Quantum efficiency of Group 3 SSPMs as a function of bias.

4.3.2 Bias Current

The bias current through detectors from each of the three epitaxy groups was measured as a function of temperature and bias voltage under low background ($\Phi < 5 \times 10^6$ photons/cm^2-s) conditions. Data from a representative 200 x 200 μm^2 SSPM from each group was gathered and is shown in Table VI and plotted in Figures 16, 17 and 18. As expected, the bias current varied roughly exponentially with reciprocal temperature and bias voltage. The bias current I_{bias} is approximately

$$I_{bias}(V,T) = C_1 A \exp(C_2 V + C_3/T),$$

where A is the detector area and C_1, C_2 and C_3 are constants which depend on the doping levels and profiles used in a particular device. The effect of field-assisted thermal ionization and the SSPM doping profiles can cause changes in the detectors' electric field profiles at different biases. This can result in a departure from the exponential dependence at lower bias voltages.

It is important to note that the carriers responsible for the steady-state bias current were not subject to the full SSPM gain due to the structure of the detectors. The dark current had very low noise as a result, and SSPM pulses due to detected photons or occasional dark counts stood out well above this noise.

Table VI. Bias current density (pA/mil^2) for SSPMs at various temperatures and bias voltages ($\Phi < 5 \times 10^6$ ph/cm^2-s)

Bias (V)	Temp (K)	Epitaxy Group: Group 1	Group 2	Group 3
6.0	6	10.1	4.4	2.9
6.2	6	13.0	5.8	4.4
6.4	6	14.5	7.2	4.4
6.6	6	17.4	7.2	5.8
6.8	6	21.7	8.7	7.2
7.0	6	-	10.1	8.7
7.2	6	-	11.7	8.7
7.4	6	-	13.0	10.1
7.6	6	-	15.9	11.7
6.0	7	40.5	20.3	11.7
6.2	7	47.8	24.6	13.0
6.4	7	57.9	27.5	15.9
6.6	7	69.5	31.9	18.8
6.8	7	81.0	36.2	21.7
7.0	7	-	42.0	24.6

Table VI. (Continued)

Bias (V)	Temp (K)	Epitaxy Group: Group 1	Group 2	Group 3
7.2	7	-	47.8	29.0
7.4	7	-	55.0	34.7
6.0	8	121.6	63.7	29.0
6.2	8	143.2	75.2	36.2
6.4	8	170.7	85.4	37.6
6.6	8	201.1	98.4	42.0
6.8	8	231.5	112.9	49.2
7.0	8	-	127.3	56.4
7.2	8	-	143.2	65.1
6.0	9	280.7	156.3	33.3
6.2	9	332.8	179.4	40.5
6.4	9	392.1	205.5	49.2
6.6	9	458.6	233.0	60.8
6.8	9	-	264.8	72.4
7.0	9	-	296.6	85.4
7.2	9	-	332.8	101.3
6.0	10	548.3	308.2	70.9
6.2	10	643.8	354.5	85.4
6.4	10	748.0	400.8	101.3
6.6	10	853.6	455.8	123.0
6.8	10	-	510.7	147.6
7.0	10	-	572.9	175.1
7.2	10	-	638.0	-
6.0	11	1017.1	559.9	182.3
6.2	11	1167.6	640.9	218.5
6.4	11	1328.1	732.1	259.0
6.6	11	1494.5	827.6	301.0
6.8	11	-	918.7	351.6
7.0	11	-	1011.3	408.0

-After Breakdown

4.3.3 Recommended Operating Conditions

For the devices fabricated and characterized in this study, the recommended operating temperature is 10 K. To maximize quantum efficiency at this temperature, the highest bias voltage that can be applied without a significant risk of overloading the device is 7.0 V, for the SSPMS from epitaxy Group 2.

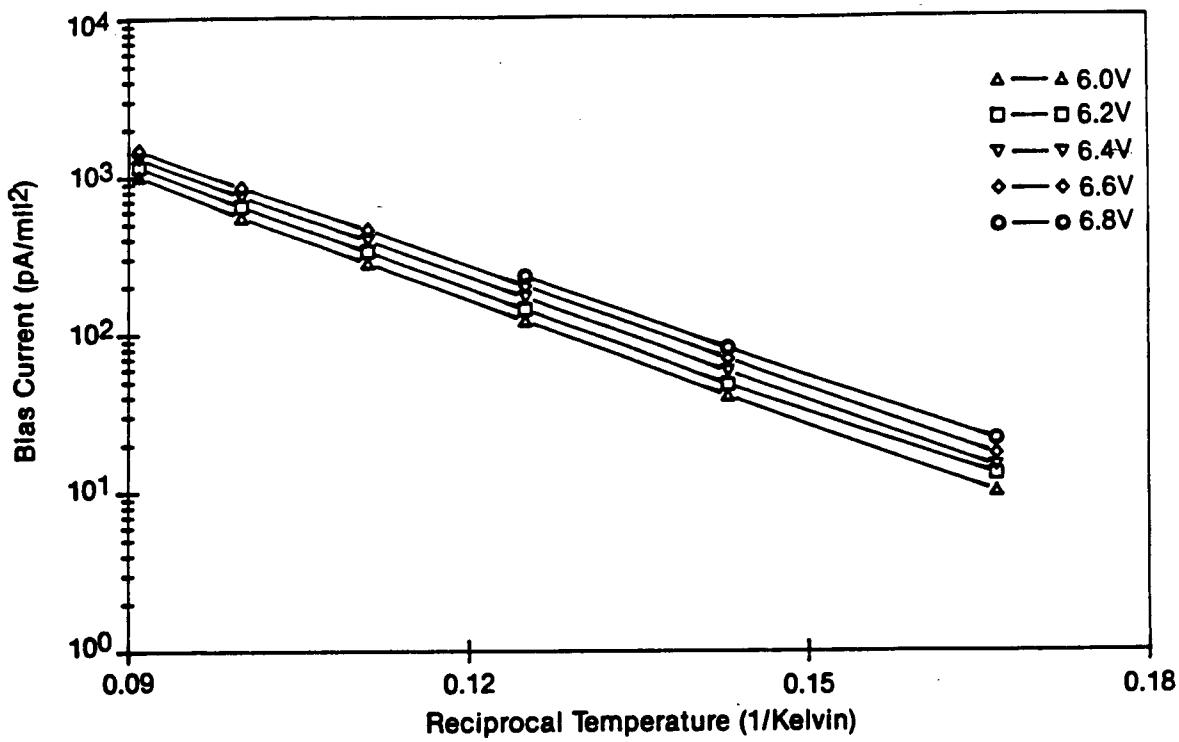

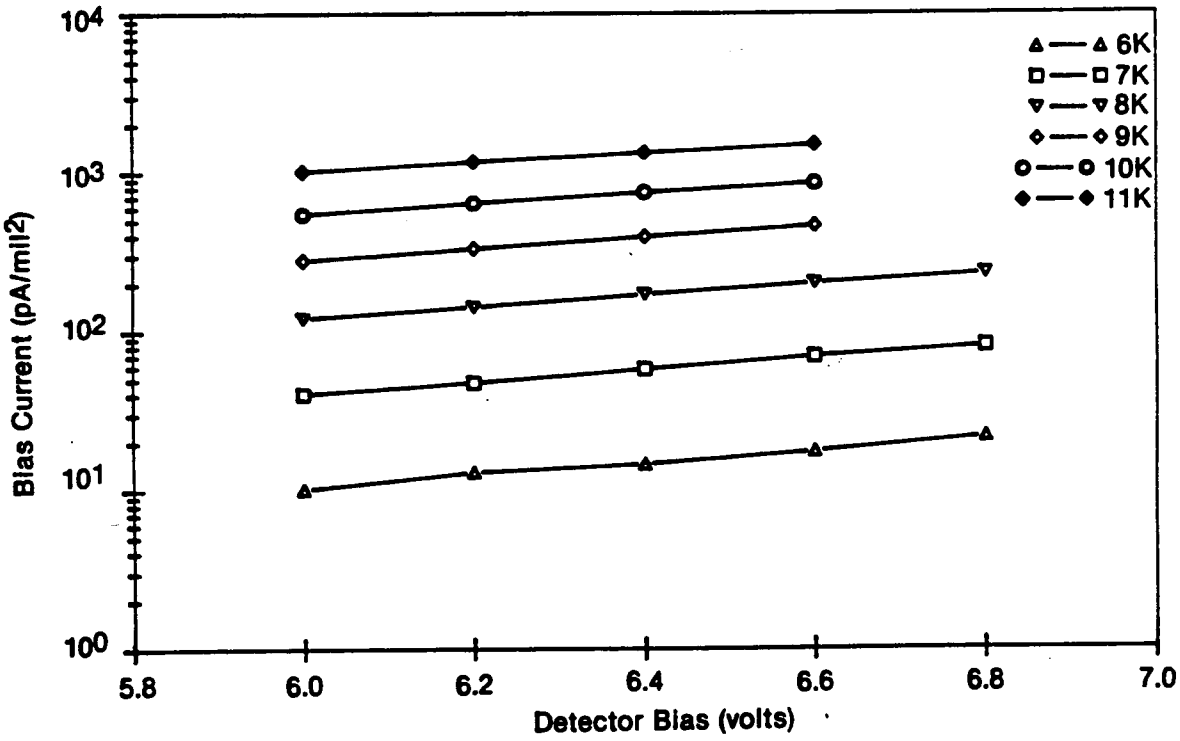

Figure 16. Bias current of Group 1 SSPMs as a function of bias voltage and temperature.

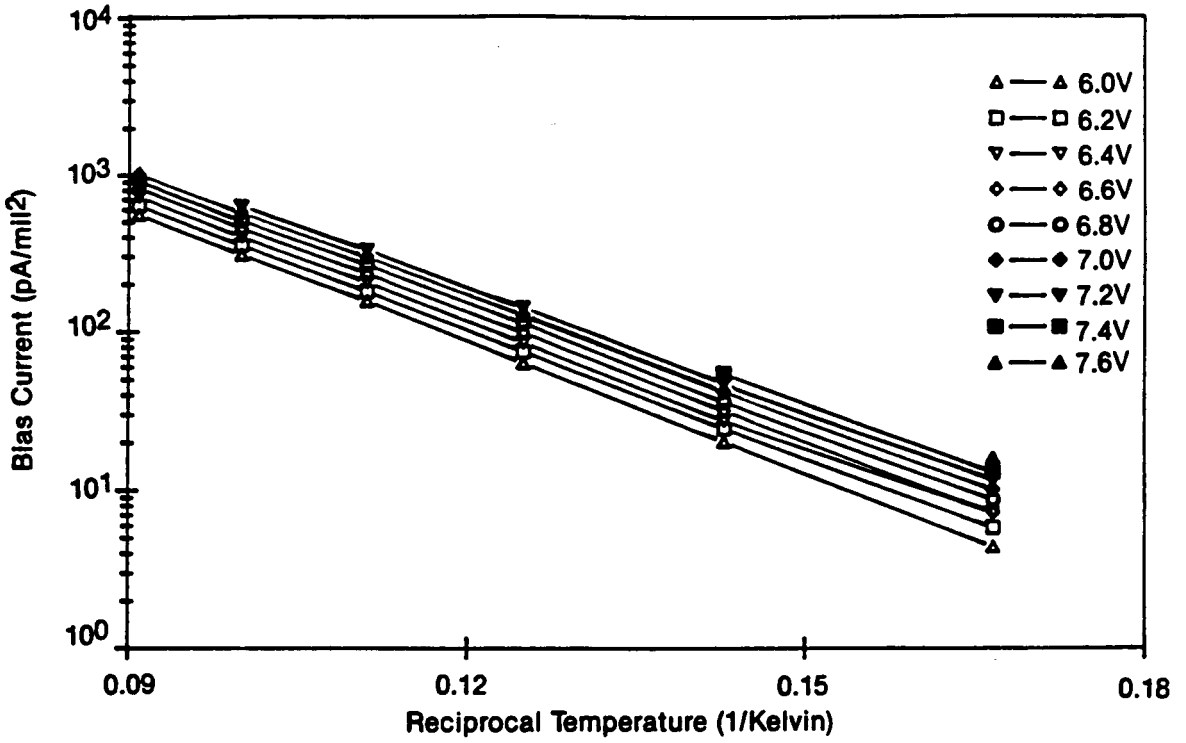

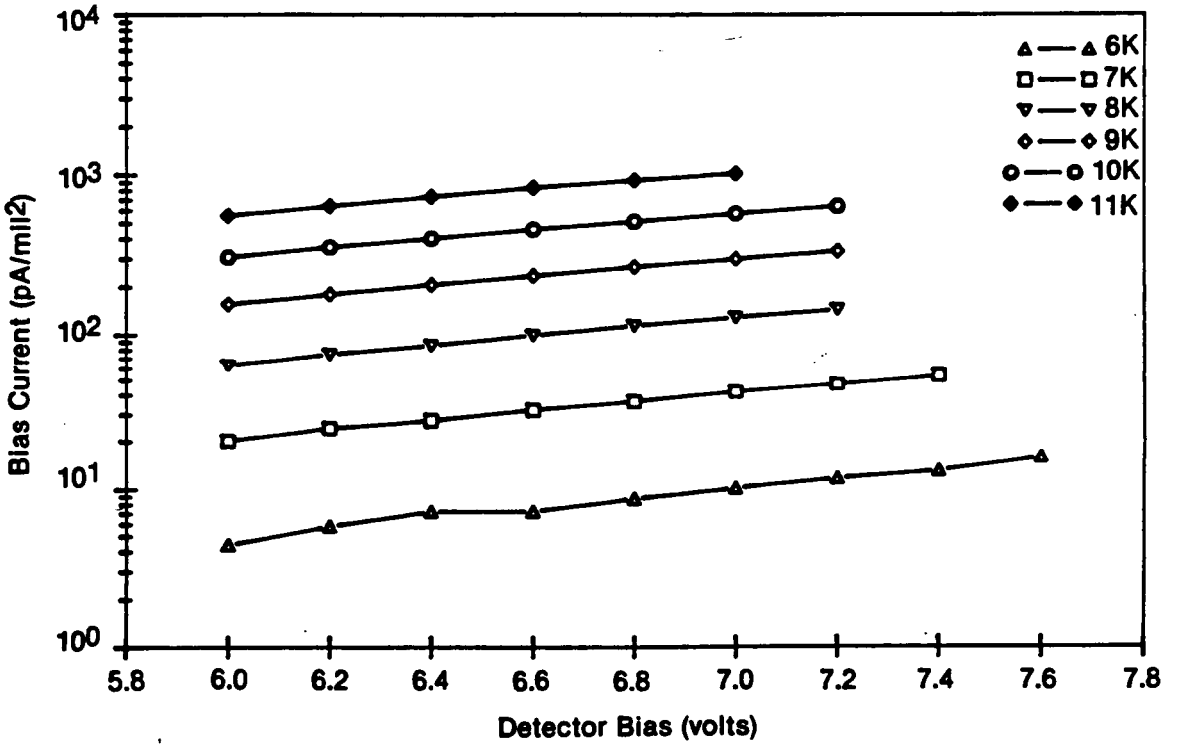

Figure 17. Bias current of Group 2 SSPMs as a function of bias voltage and temperature.

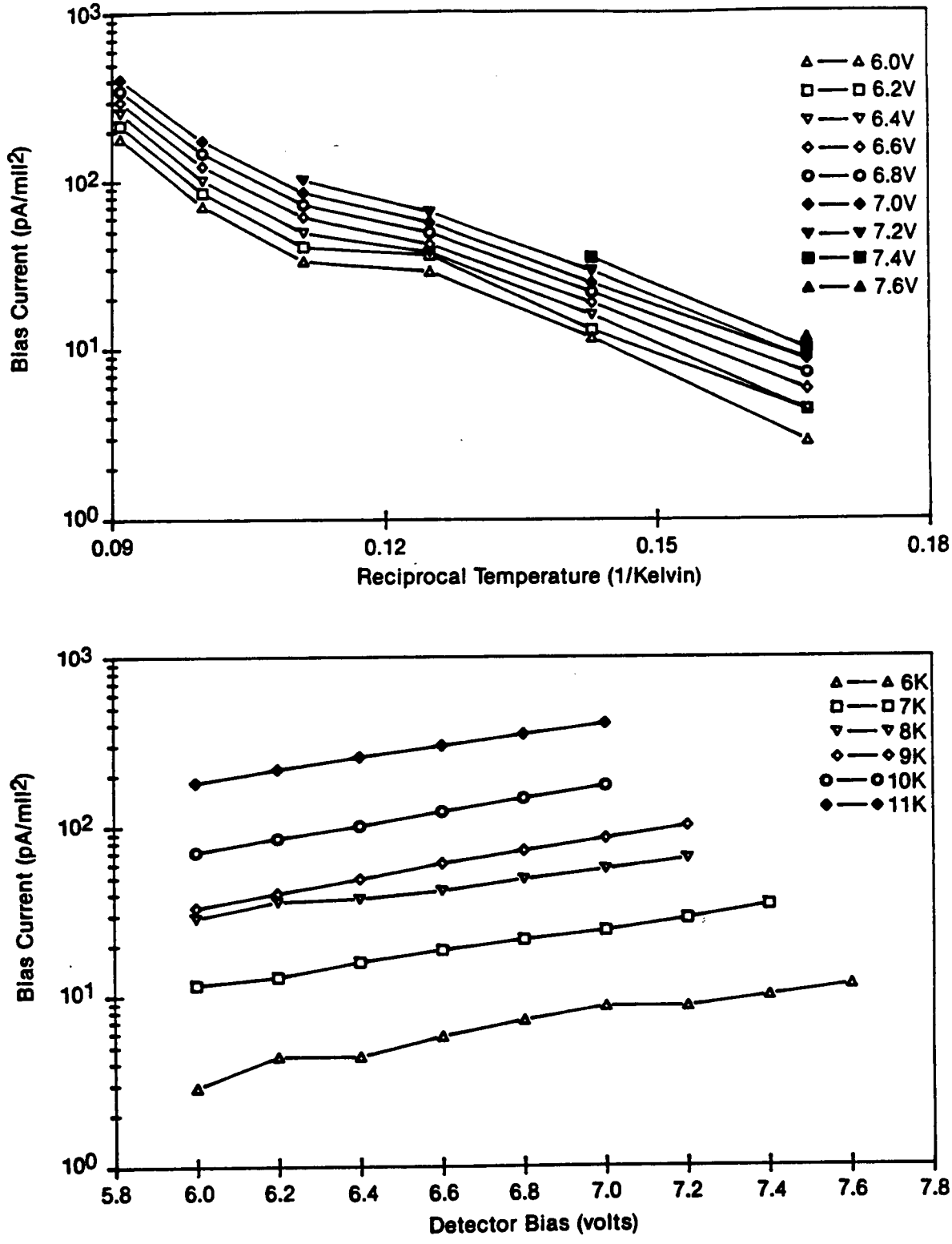

Figure 18. Bias current of Group 3 SSPMs as a function of bias voltage and temperature.

Since these detectors function as high-impedance devices that emit sharp current pulses, their outputs should first be processed through a transimpedance preamplifier. Care should be taken to keep stray capacitance between the SSPM and the preamplifier below a few tens of picofarads in order to avoid attenuating the SSPM pulse amplitudes.

4.4 TASK ASSESSMENT

A processing lot of SSPMs was fabricated and characterized, with emphasis on conditions suitable for space-based astronomy applications. Three different epitaxial material variations were incorporated in the device lot. One of these variations produced devices superior in performance to any previously produced. For these devices, the recommended operating temperature is 10 K. To maximize quantum efficiency at this temperature, the highest bias voltage that can be applied without a significant risk of overloading the device is 7.0 V.

5.0 CONCLUSIONS AND RECOMMENDATIONS

Significant progress in SSPM performance improvement has been demonstrated by the devices fabricated on this program. The device fabrication lot consisted of three epitaxial material variations. Data were obtained on quantum efficiency, dark current and bias current. The temperature for optimal device performance has been increased from 7 to 10 K, and the new devices exhibit a combination of lowest dark current and highest quantum efficiency ever obtained, by a significant margin.

It is recommended that the devices showing the best potential for meeting performance goals germane to NASA applications be subjected to detailed characterization. Dark count rates should be measured as a function of temperature and bias voltage and the spectral dependence of the quantum efficiency for low flux levels should be measured as a function of temperature and bias voltage. Data on average SSPM gain as a function of absorbed photon flux is useful in determining the dynamic range of the SSPM. Measurements of detector parameters as a function of detector area provide a relationship between designed and effective detector areas, which will be useful in establishing future device design rules.

Device modeling of SSPM performance is proceeding along the direction recommended in the previous report[3] viz, treatment of the electron avalanche process via the Boltzmann equation. Formulation of theory and setup of the computer codes for equation solution are being performed on another program[4] and the required simulations are being performed on the ARC CRAY XMP supercomputer. Some initial results have been obtained on the single-electron transport theory. These were limited since the communications link between the Science Center and NASA-ARC did not become operational until late in this phase of the contract. It is recommended, now that the link is complete, that simulation of the single- and multiple-electron theories and improvement of the neutral-impurity scattering theory be performed on the ARC supercomputer.

6.0 REFERENCES

[1] M. D. Petroff, M. G. Stapelbroek and W. A. Kleinhans, U. S. Patent Number 4,586,068, Filed Oct. 7, 1983, Granted Apr. 29, 1986.

[2] M. D. Petroff, M. G. Stapelbroek and W. A. Kleinhans, Appl. Phys. Lett. 51 (1987) 406.

[3] Study of Solid State Photomultiplier, NASA Contractor Report No. CR177465, August 1987.

[4] Solid State Photomultiplier Technology Development, Contract No. F33615-87-C-1447. Issued by the USAF Systems Command, Wright-Patterson AFB, M. Dodd, Project Engineer.

[5] R. A. LaViolette and M. G. Stapelbroek, J. Appl. Phys. (submitted March 15, 1988).

[6] The modifications to accommodate hole transport are straightforward and parallel the discussion devoted herein to electrons.

[7] J. M. Ziman, Principles of the Theory of Solids, 2nd ed. (Cambridge University, 1979).

[8] Lord Kelvin, Phil Mag. 2 (1901) 1.

[9] J. R. Barker, J. Phys. C 6 (1973) 2663.

[10] S. K. Sarker, J. H. Davies, F. S. Khan and J. W. Wilkins, Phy. Rev. B33 (1986) 7263.

[11] W. Fawcett, A. D. Boardman and S. Swain, J. Phys. Chem. Solids 31 (1970) 1963.

[12] C. Jacoboni and L. Reggianiani, Rev. Mod. Phys. 55 (1983) 645.

[13] Phonon absorption might be considered for a germanium-based SSPM, however.

[14] This extension of the long-wavelength response of the SSPM has not been explained and is the subject of a proposal originally submitted to the Army Research Office (February, 1988).

[15] G. Wannier, Phys. Rev. 90 (1953) 817.

[16] C. Erginsoy, Phys. Rev. 79 (1950) 113.

[17] L. E. Blagosklonskaya, E. M. Gershenzon, Y. P. Ladyzhinskii and A. P. Popova, Sov. Phys. Solid State 11 (1970) 2402.

[18] B. K. Ridley, Quantum Processes in Semiconductors (Oxford University, 1982).

[19] J. Callaway, Phys. Rept. 45 (1978) 89.

[20] Y.C. Chang, T. C. McGill and D. L. Smith, Phys. Rev. B 23 (1981) 4169.

[21] R. S. Klein, Characterization and Modeling of BIB Detectors using Capacitance versus Voltage Measurements, IRIA-IRIS, Proceedings of the Meetings of the Specialty Group on Infrared Detectors (Boulder, CO, August 1985).

NASA
National Aeronautics and Space Administration

Report Documentation Page

1. Report No.	2. Government Accession No.	3. Recipient's Catalog No.
NASA CR-177514		

4. Title and Subtitle
Solid State Photomultiplier for Astronomy (U) - Phase II

5. Report Date
May 1989

6. Performing Organization Code

7. Author(s)
P.J. Besser, K.M. Hays, R.A. La Violette

8. Performing Organization Report No.

10. Work Unit No.
506-45-31

9. Performing Organization Name and Address
Rockwell International Science Center
3370 Miraloma Ave., Mail Code 031-BA13
P.O. Box 3105
Anaheim, CA 92803

11. Contract or Grant No.
NAS2-12400

13. Type of Report and Period Covered
Contractor Report
Sept. 30-June 10, 1988

12. Sponsoring Agency Name and Address
NASA Ames Research Center
Mail Stop 244-10
Moffett Field, CA 94035

14. Sponsoring Agency Code

15. Supplementary Notes
Technical Monitor: John H. Goebel
NASA Ames Research Center
Mail Stop 244-10
Moffett Field, CA 94035
(415) 694-3188 or (FTS) 464-3188

16. Abstract

Epitaxial layers with varying donor concentration profiles were grown on silicon substrate wafers using chemical vapor deposition (CVD) techniques, and Solid State Photomultiplier (SSPM) devices were fabricated from the wafers. Representative detectors were tested in a low background photon flux, low temperature environment to determine the device characteristics for comparison to NASA goals for astronomical applications. SSPM temperatures varied between 6 and 11 K with background fluxes in the range from $< 5 \times 10^{6}$ to 10^{13} photons/cm ^{2} -s at wavelengths of 3.2 and 20 cm. Measured parameters included quantum efficiency, dark count rate and bias current. Temperature for optimal performance is 10 K, the highest ever obtained for SSPMs. The devices exhibit a combination of the lowest dark current and highest quantum efficiency yet achieved. Experimental data were reduced, analyzed and used to generate recommendations for future studies.

The background and present status of the microscopic theory of SSPM operation were reviewed and are summarized. Present emphasis is on modeling of the avalanche process which is the basis for SSPM operation. Approaches to the solution of the Boltzmann transport equation are decribed and the treatment of electron scattering mechanisms is presented. The microscopic single-electron transport theory is ready to be implemented for large-scale computations. Future work will be directed towards simulation of the multi-electron theory, improvement of the neutral-impurity scattering theory and consideration of other scattering mechanisms.

17. Key Words (Suggested by Author(s))	18. Distribution Statement
Infrared Detectors Infrared Technology Photon Detectors	Unclassified - Unlimited Subject Category 35

19. Security Classif. (of this report)	20. Security Classif. (of this page)	21. No. of pages	22. Price
Unclassified	Unclassified	43	A03